Supplementary Information

Electronic Tuning of Dynamic Imine Bonds Enables Programmable Pore Gating in Metal–Organic Frameworks

Meng Qiao[1,3†], Youcong Li[2,†], Shengcun Chen[3], Sirui Liu[3], Yuhao Gu[2], Dong Zhang[2], Yifan Liu[2], Lei Gao[2], Mengting Chang[3], Xing Zhang[3,*], Shuai Yuan[2,*]

[1] Research Center of Pharmaceutical and Synthetic Biology/Department of Food Nutrition and Safety, College of Engineering, China Pharmaceutical University, Nanjing 211198, China

[2] State Key Laboratory of Coordination Chemistry, School of Chemistry and Chemical Engineering, Nanjing University, Nanjing, Jiangsu, 210023, China

[3] State Key Laboratory of Microbial Technology, School of Food Science and Pharmaceutical Engineering, Nanjing Normal University, Nanjing 210023, China

[†]These authors contributed equally to this work.

*Correspondence: zhangxing@njnu.edu.cn; syuan@nju.edu.cn

Experimental Section

Synthesis of H_2AZDC (azobenzene-4,4'-dicarboxylic acid).

The H_2AZDC was synthesized according to the previously reported method with slight modification. In a 500 mL flask, 11 g *p*-nitrobenzoic acid and 40 g sodium hydroxide were dissolved in 150 mL of deionized water. The mixture was maintained at 50°C in a water bath. Separately, 90 g glucose was dissolved in 100 mL of deionized water at 65°C, and the resulting solution was added dropwise to the flask over 1 h. The mixture was bubbled with oxygen under continuous stir overnight, followed by the addition of 50 mL methanol. The precipitate was collected by filtration, washed with 1 L of methanol, and dried under vacuum for 24 h. The dried solid was redissolved in 400 mL of deionized water at 50 °C and acidified with 10% HCl aqueous solution. Finally, the product was collected by centrifugation and washed repeatedly with deionized water until the supernatant appeared near-colorless.

Single-crystal X-ray diffraction.

Diffraction data collection. SCXRD data were collected on a Bruker D8 Venture diffractometer fitted with monochromatized microfocus Ga-Kα radiation (λ = 1.34139 Å) and PHOTON-100 CMOS detector. The crystal was kept at 193 K with a nitrogen flow controlled by a KRYOFLEX II low temperature attachment. Raw data collection and reduction were performed using APEX3 software. Absorption corrections were applied using the SADABS routine.

Structure determination and refinement. The structures were solved by intrinsic phasing with the SHELXT4 structure solution program and refined by full-matrix least-squares on F2 with the SHELXL5 refinement package in the Olex26 software package. All non-hydrogen atoms were refined with anisotropic displacement parameters. All hydrogen atom positions were added to their mother atoms by geometry and refined by a riding model. SIMU, ISOR, SADI, DFIX, DANG, and FLAT restraints were used to obtain reasonable parameters. The free solvent molecules of DMF in the void space

were highly disordered and unable to be located and refined, and were removed using the solvent mask in Olex2. The contents of the solvent and counterions are not represented in the unit cell contents in the final crystal data.

Crystal structure information. The crystal data and details of the structure refinements are given in Tab. S2-4. CCDC 2538814-2538822 contain the supplementary crystallographic data for this paper. The data can be obtained free of charge from the Cambridge Crystallographic Data Centre via www.ccdc.cam.ac.uk/data_request/cif.

Preparation of paclitaxel@PCN-160-X. First, the synthesized PCN-160-X needs to be washed three times with DMSO to completely remove residual DMF. After that, 0.75 mg of the treated MOF was incubated with a paclitaxel solution at room temperature for 12 h, where paclitaxel was dissolved in a mixture of DMSO and deionized water (2:1 v/v). Similarly, other drug@PCN-160-X composites were prepared using the same method.

Study of the drug adsorption and release.

Drug adsorption. 0.75 mg of washed MOF was incubated with paclitaxel solution at room temperature. Samples were rotated on a longitudinal axis rotator at 30 rpm for 12 h. Aliquots (5 μL of supernatant) were collected at specified time intervals. Paclitaxel concentration was quantified by HPLC. All adsorption tests were performed in triplicate with mean values reported.

Drug release. The drug release profile of paclitaxel@PCN-160-X was investigated *in vitro*. Following composites preparing, samples were immersed in 200 μL of PBS (pH 7.4). Aliquots (20 μL of supernatant) were collected at predetermined time intervals, and the paclitaxel concentration was quantified by HPLC. All release experiments were performed in triplicate, and data are reported as mean values.

HPLC analysis for paclitaxel. HPLC analysis was performed on an Agilent 1260 Infinity II LC system equipped with an HPLC C18 column (Pursuit 5 C18, 250 × 4.6 mm, Agilent, US) at 35 °C. Eluent A was 0.1% trifluoroacetic acid (v/v) in water, and eluent B was isopropanol. An 10% amount of eluent A was flowed (0.6 mL/min) through the column for 15 min. The column effluent was continuously detected by PDA at 262 and 310 nm.

Cell Culture. Human breast cancer cells (MCF-7) were cultured in the RPMI 1640 medium with penicillin and streptomycin at 37 ℃ in a 5% CO_2 incubator.

Cytotoxicity study (MTT assay). For the cell viability, MCF-7 cells were harvested by trypsinization and resuspended at a concentration of $2*10^4$ cells/mL in fresh culture medium. Then, the cells were seeded at a density of 5000 cells/well in 96-well plates. After 24 h of incubation at 37℃ with 5% CO_2, the culture medium was replaced with 200 mL of medium containing one of the three drug samples, free paclitaxel, PCN-160-X, paclitaxel@PCN-160-X. The amount of the drugs ranged from 0.1 mg to 0.5 mg. After 24 h of incubation, the drug-containing media were abandoned, and 20 μL of MTT (5 mg/mL) solution was added to each well. The plate was incubated for an additional 4 h, and then, 200 mL of DMSO was added to each well to dissolve any formed purple formazan crystals. The plates were vigorously shaken before measuring the relative color intensity. The absorbance at 590 nm of each well was measured with a plate reader.

Apoptosis assay. Cell apoptosis was determined by an annexin V-FITC/PI apoptosis detection kit. Briefly, $1*10^5$ MCF-7 cells were plated in 6-well plates and incubated for 24 h. After exposure to the different samples (free paclitaxel, PCN-160-X, paclitaxel@PCN-160-X) for 24 h, the cells were harvested by EDTA-free trypsinization, washed in PBS twice and resuspend cells in 100 μL of 1× binding Buffer. Next, 5 μL annexin V-FITC and 10 μL PI staining solution were added and incubated in the dark for 10-15 min at room temperature. After adding 400 μL of 1× binding buffer and

mixing, samples were placed on ice and analyzed by CLSM within 1 hour. The fluorescence intensity of annexin V-FITC was measured at an excitation/emission wavelength of 488/525nm and that of PI was measured at an excitation/emission wavelength of 535/615 nm.

Figure Section

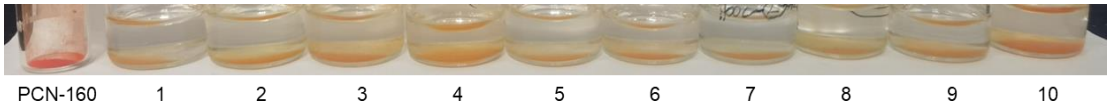

Fig. S1. The color change of the materials after the ligand exchange.

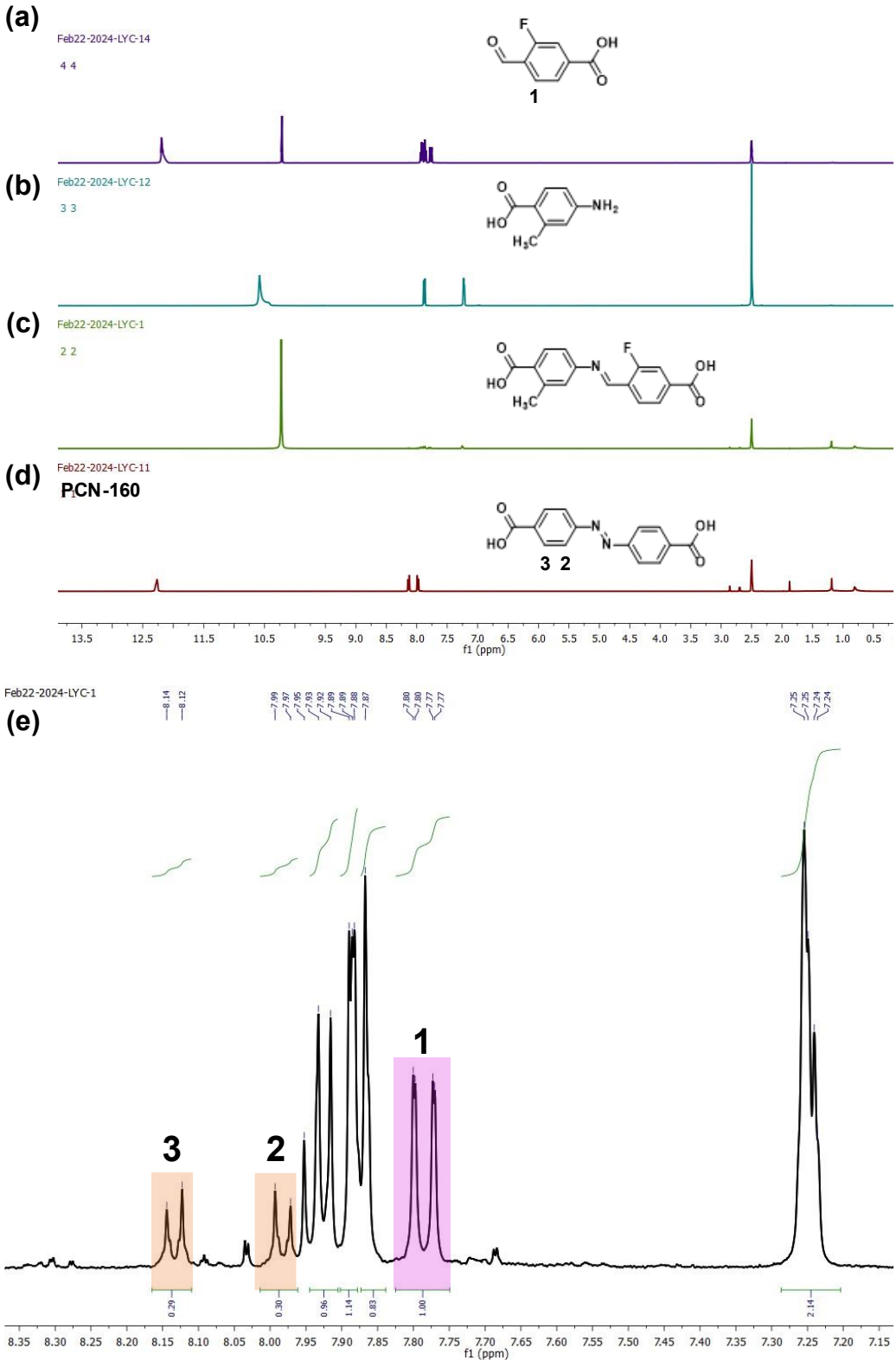

Fig. S2. ^{1}H NMR spectra of 3-fluoro-4-formylbenzoic acid (a), 4-amino-2-methylbenzoic acid (b), digested PCN-160-1 (c), digested PCN-160 (d), and enlarged version of digested PCN-160-1 (e).

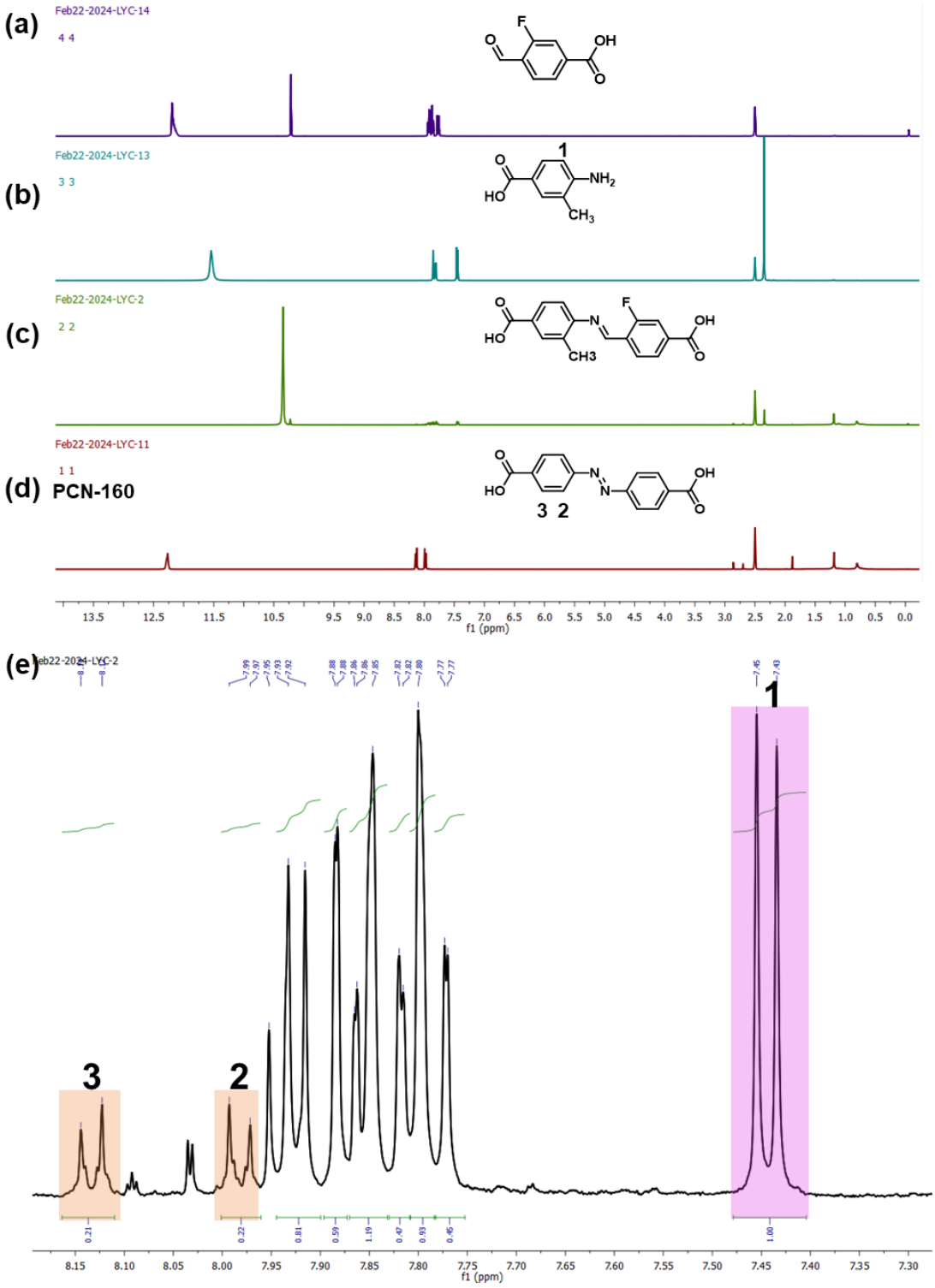

Fig. S3. ^{1}H NMR spectra of 3-fluoro-4-formylbenzoic acid (a), 4-amino-3-methylbenzoic acid (b), digested PCN-160-2 (c), digested PCN-160 (d), and enlarged version of digested PCN-160-2 (e).

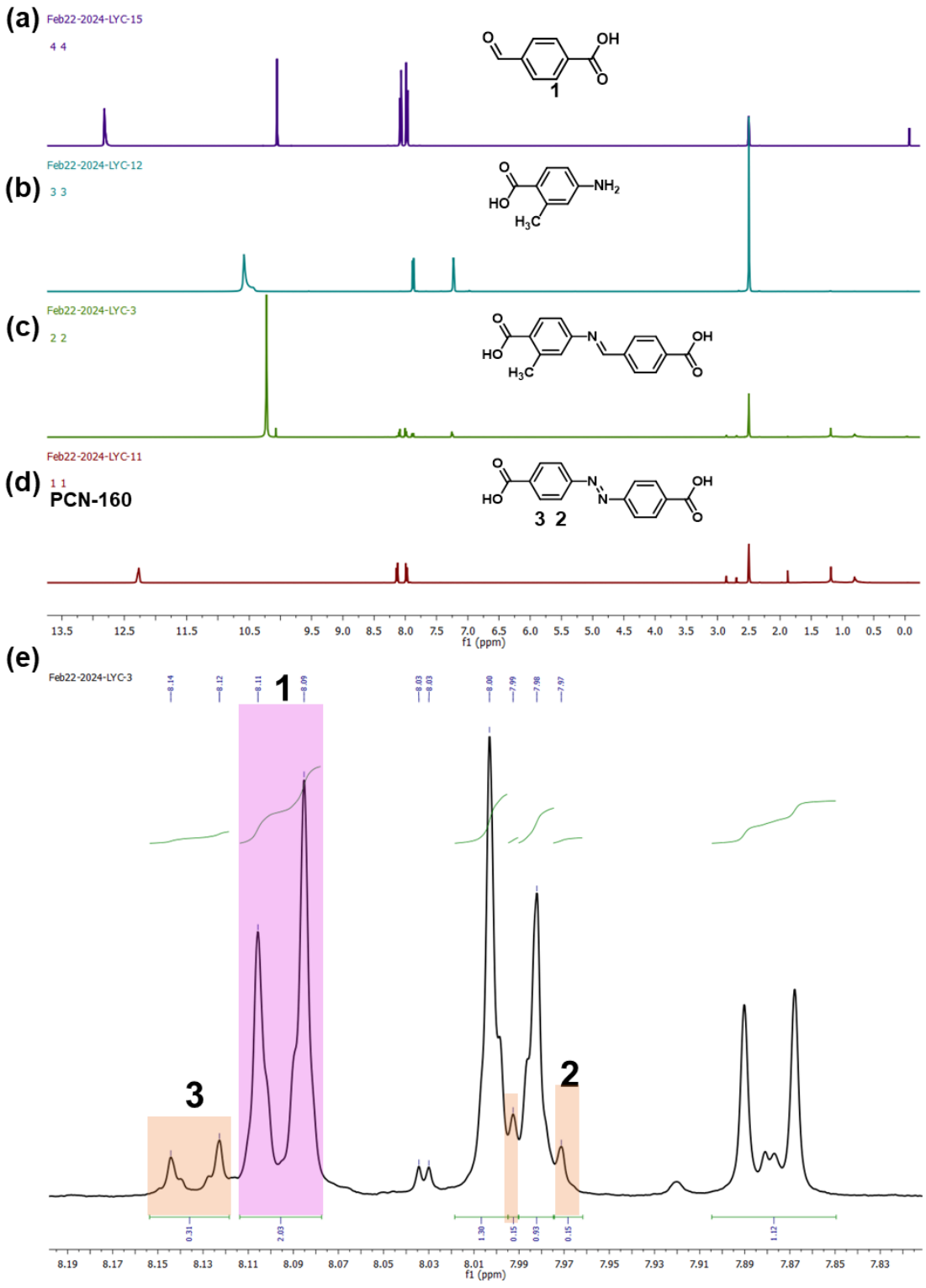

Fig. S4. ^{1}H NMR spectra of 4-formylbenzoic acid (a), 4-amino-2-methylbenzoic acid (b), digested PCN-160-3 (c), digested PCN-160 (d), and enlarged version of digested PCN-160-3 (e).

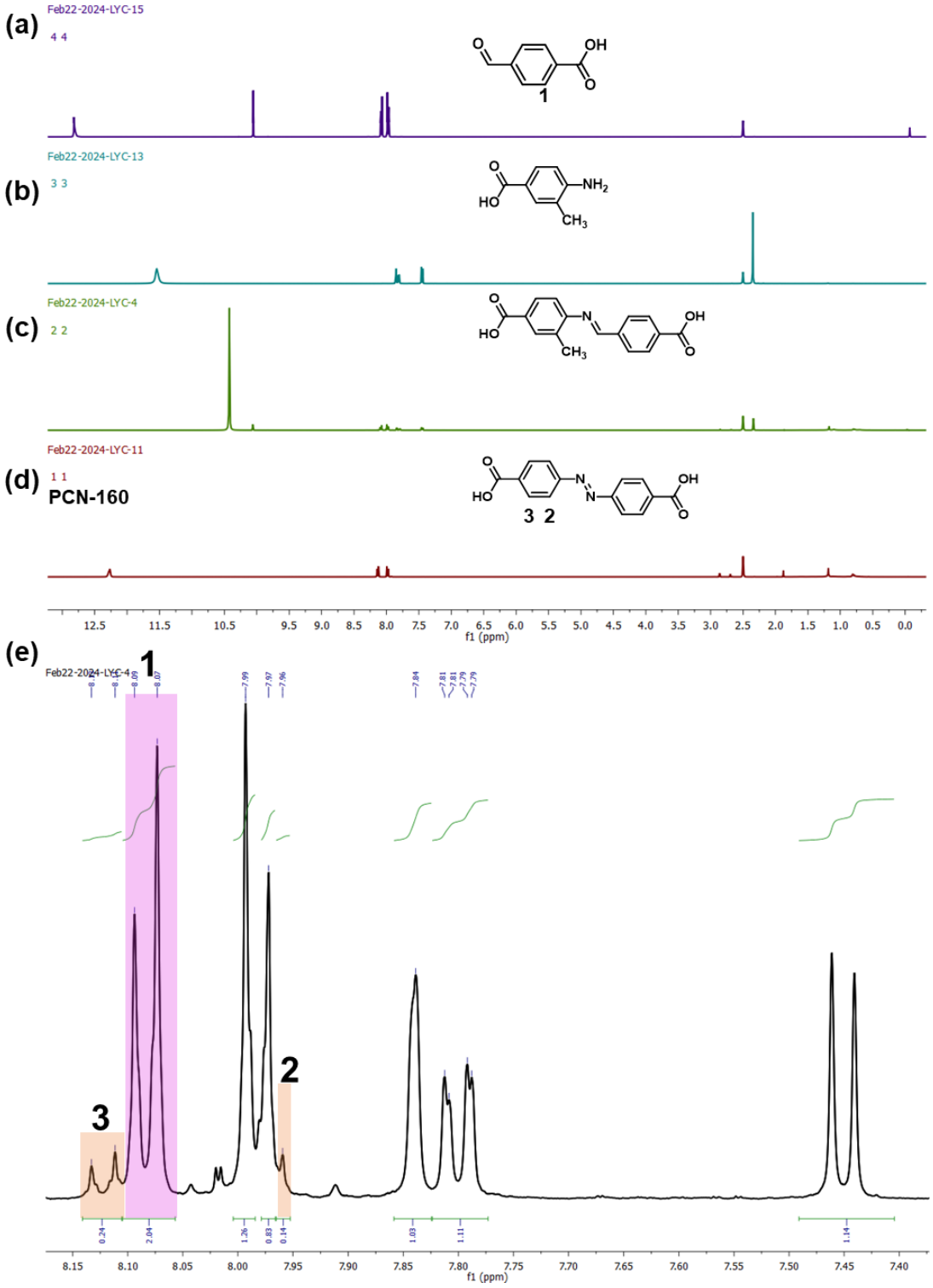

Fig. S5. ^{1}H NMR spectra of 4-formylbenzoic acid (a), 4-amino-3-methylbenzoic acid (b), digested PCN-160-4 (c), digested PCN-160 (d), and enlarged version of digested PCN-160-4 (e).

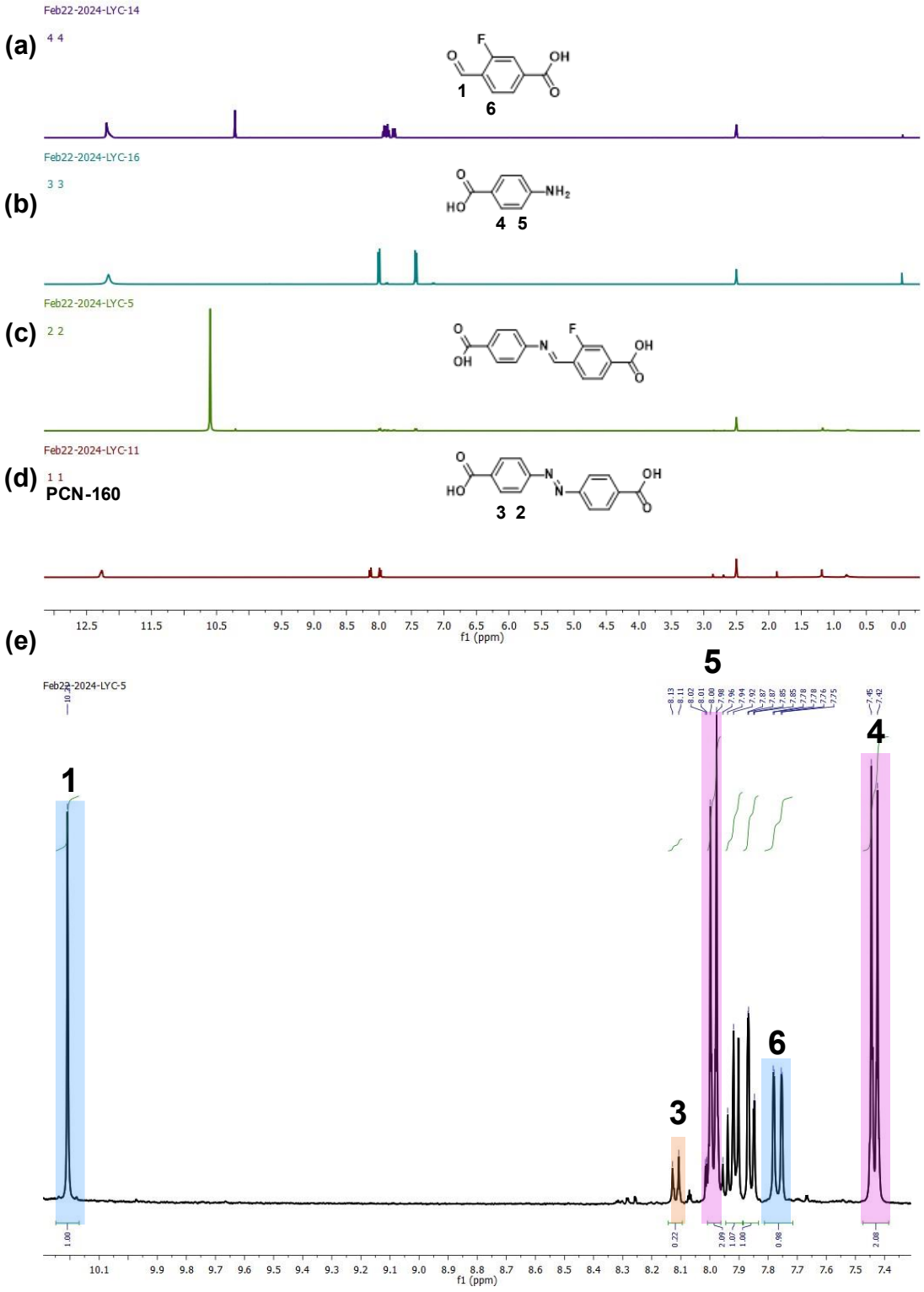

Fig. S6. ^{1}H NMR spectra of 3-fluoro-4-formylbenzoic acid (a), 4-aminobenzoic acid (b), digested PCN-160-5 (c), digested PCN-160 (d), and enlarged version of digested PCN-160-5 (e).

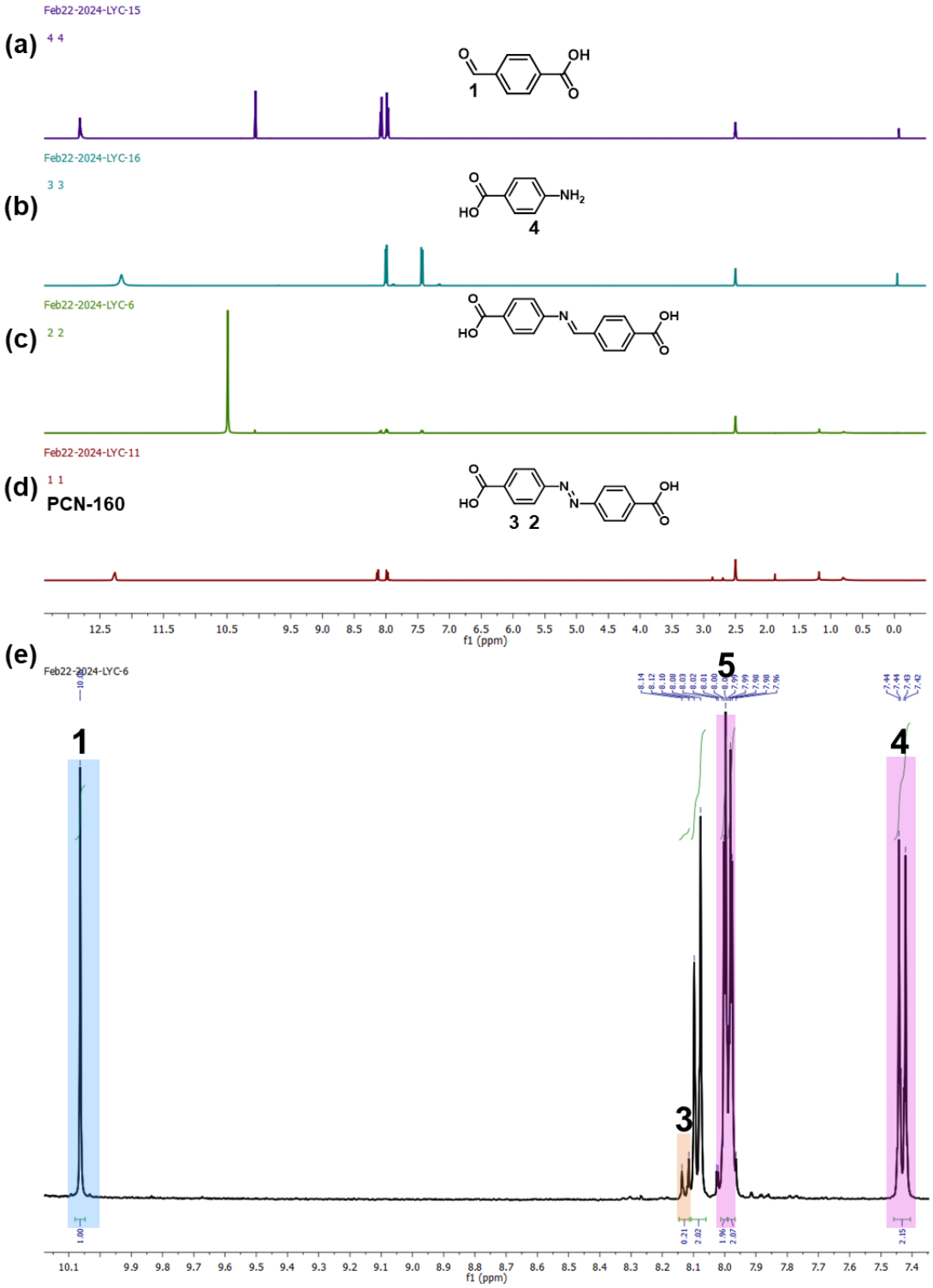

Fig. S7. ^{1}H NMR spectra of 4-formylbenzoic acid (a), 4-aminobenzoic acid (b), digested PCN-160-6 (c), digested PCN-160 (d), and enlarged version of digested PCN-160-6 (e).

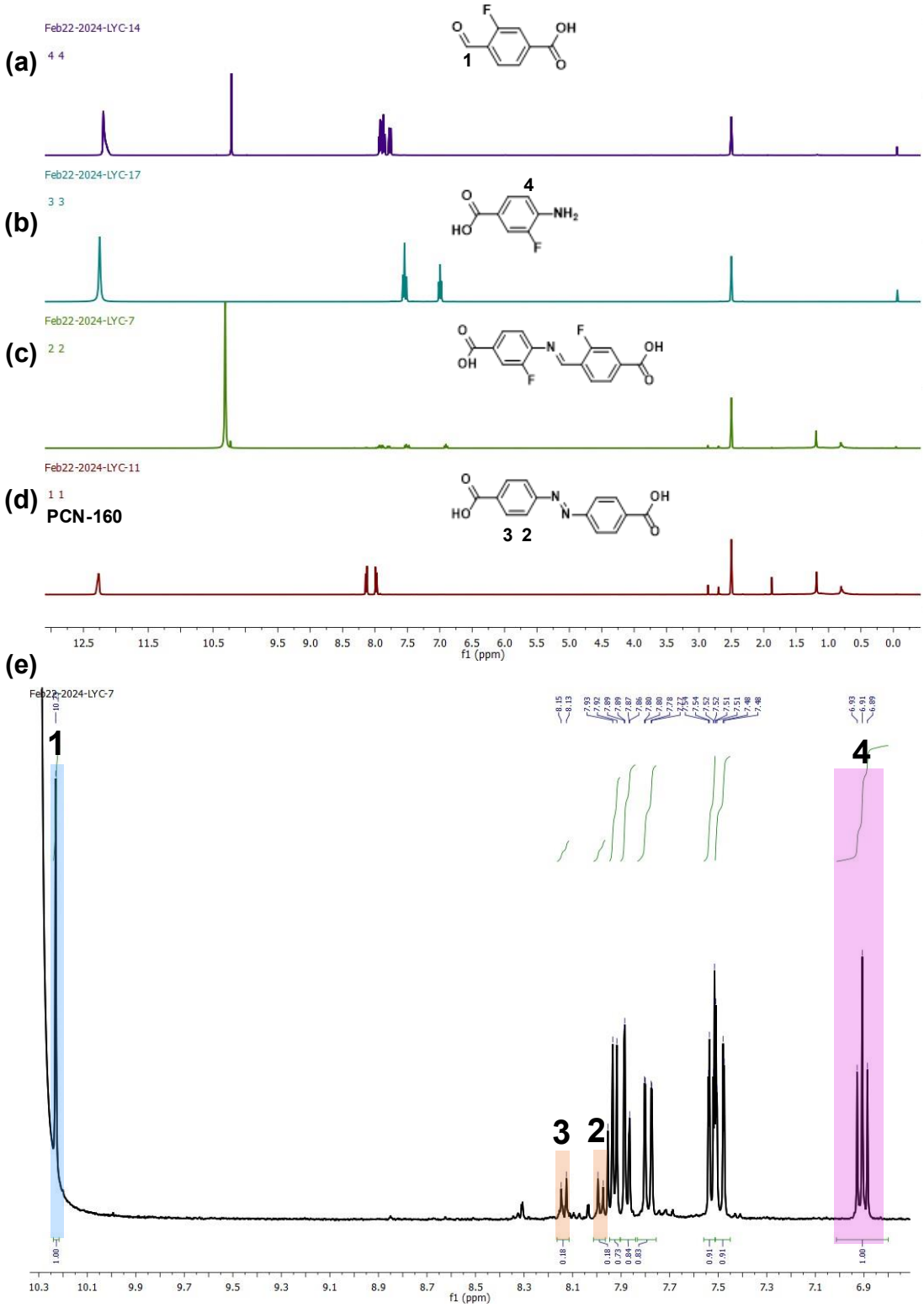

Fig. S8. ^{1}H NMR spectra of 3-fluoro-4-formylbenzoic acid (a), 4-amino-3-fluorobenzoic acid (b), digested PCN-160-7 (c), digested PCN-160 (d), and enlarged version of digested PCN-160-7 (e).

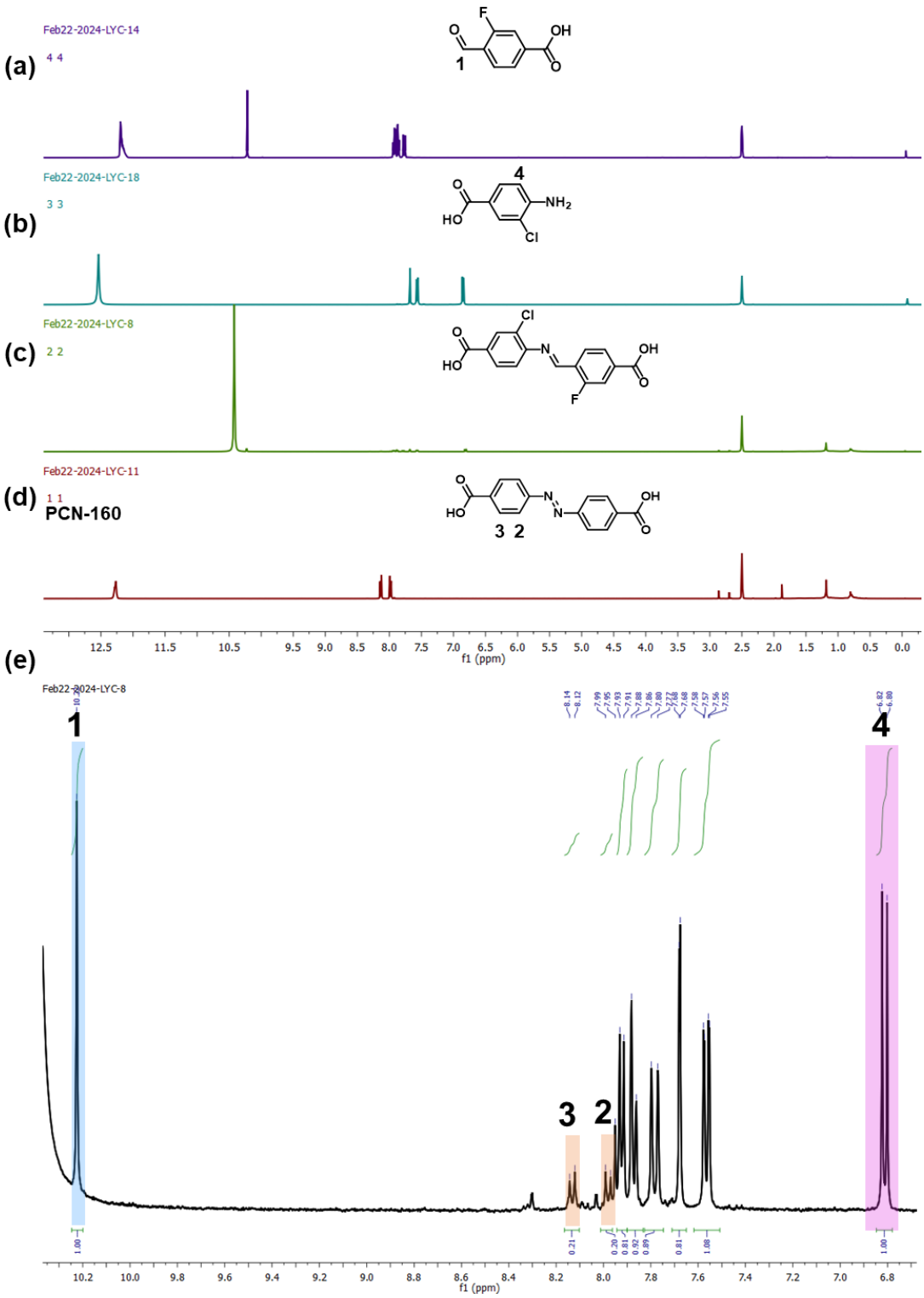

Fig. S9. ^{1}H NMR spectra of 3-fluoro-4-formylbenzoic acid (a), 4-amino-3-chlorobenzoic acid (b), digested PCN-160-8 (c), digested PCN-160 (d), and enlarged version of digested PCN-160-8 (e).

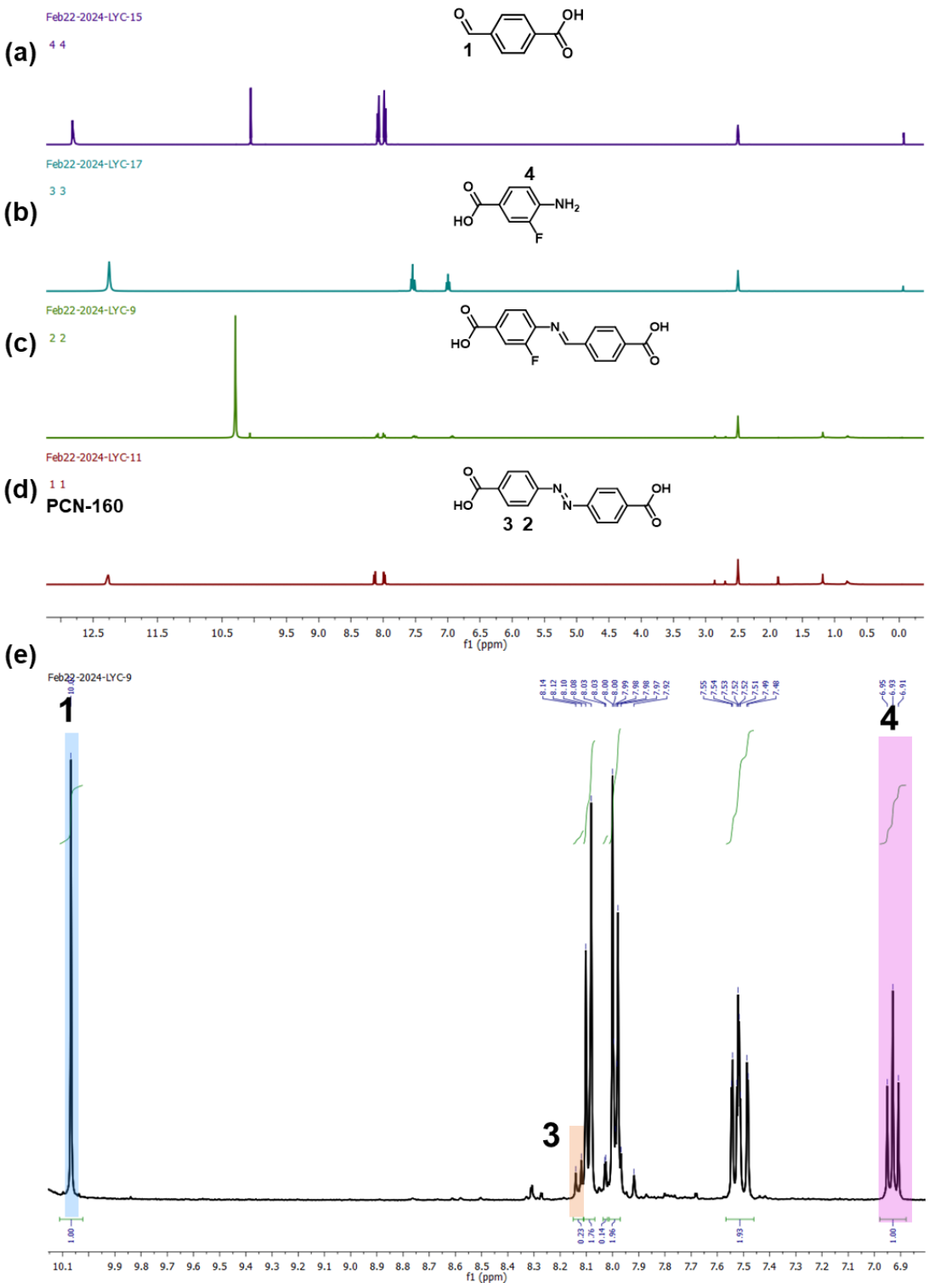

Fig. S10. ^{1}H NMR spectra of 4-formylbenzoic acid (a), 4-amino-3-fluorobenzoic acid (b), digested PCN-160-9 (c), digested PCN-160 (d), and enlarged version of digested PCN-160-9 (e).

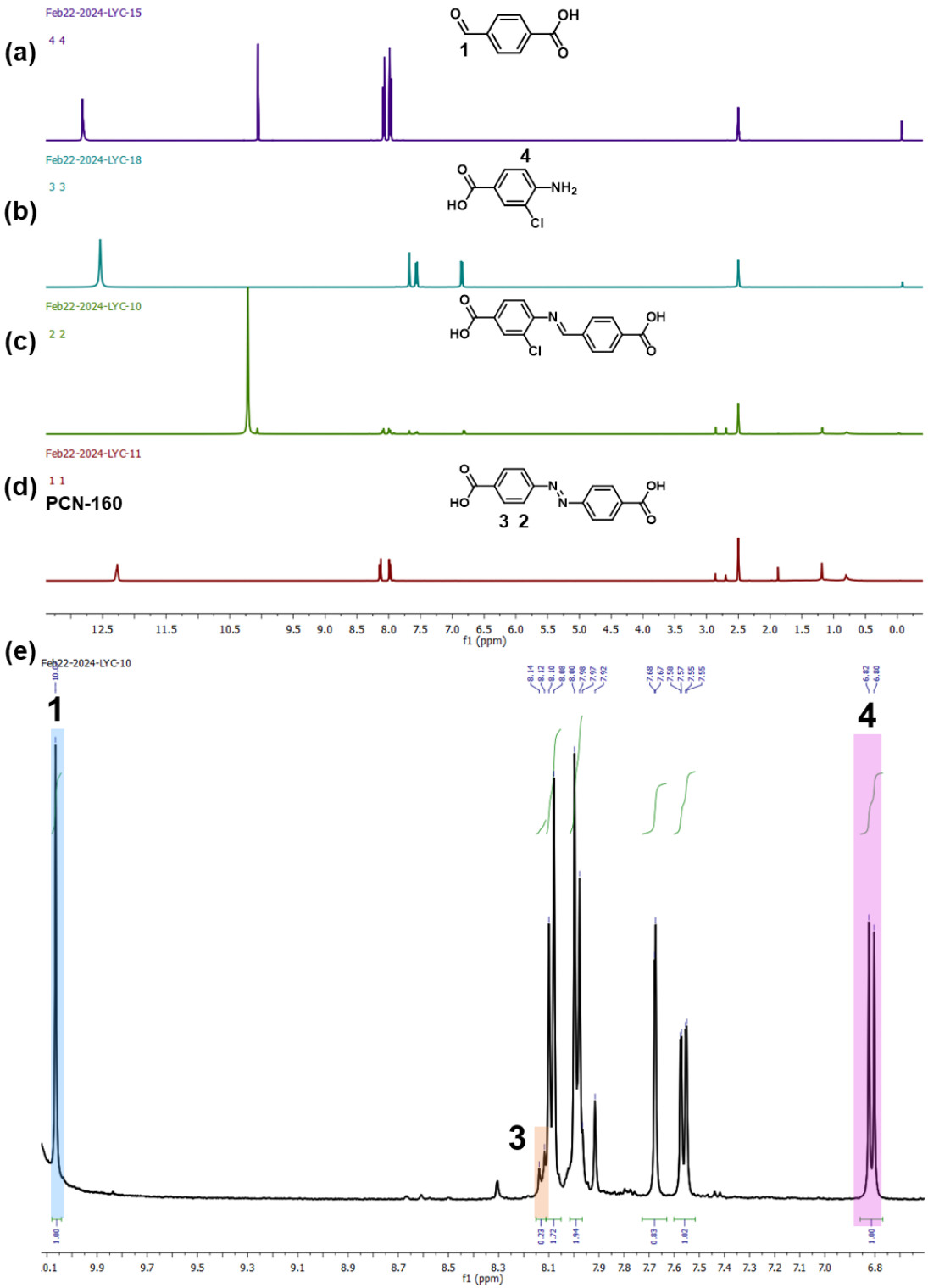

Fig. S11. ^{1}H NMR spectra of 4-formylbenzoic acid (a), 4-amino-3-chlorobenzoic acid (b), digested PCN-160-10 (c), digested PCN-160 (d), and enlarged version of digested PCN-160-10 (e).

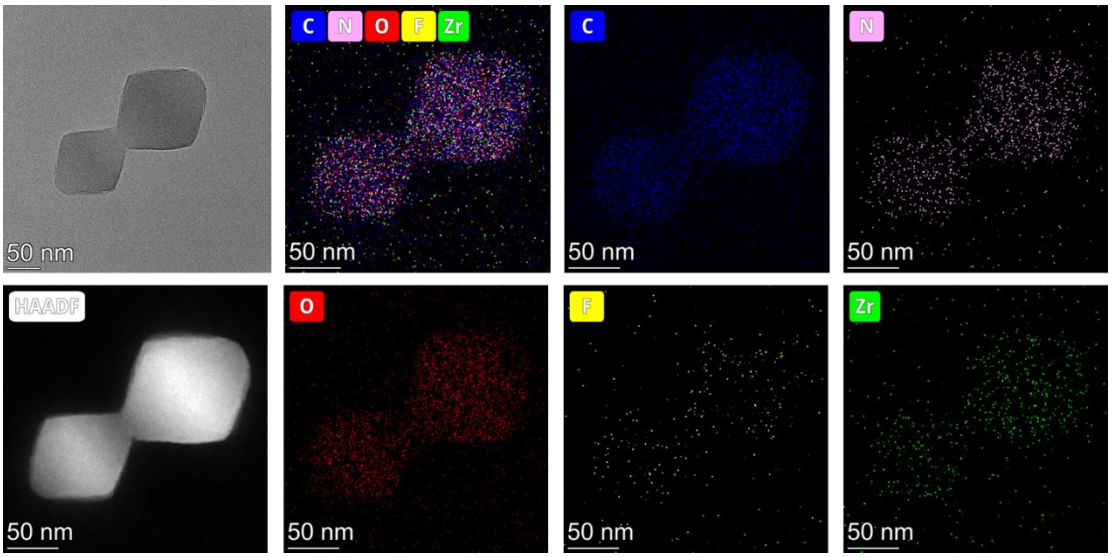

Fig. S12. TEM images and elemental mapping of PCN-160-1.

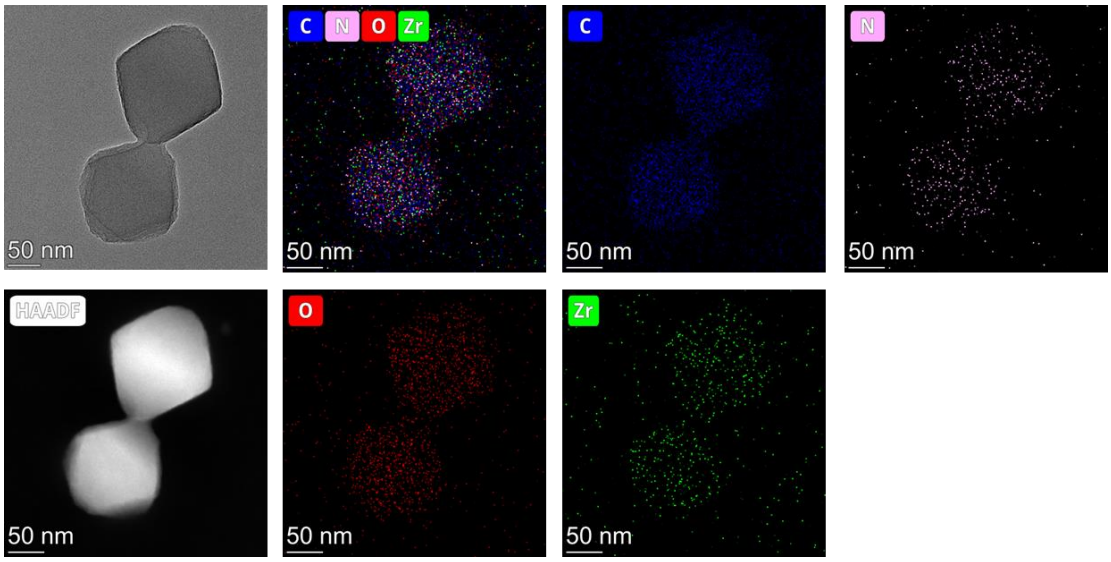

Fig. S13. TEM images and elemental mapping of PCN-160-3.

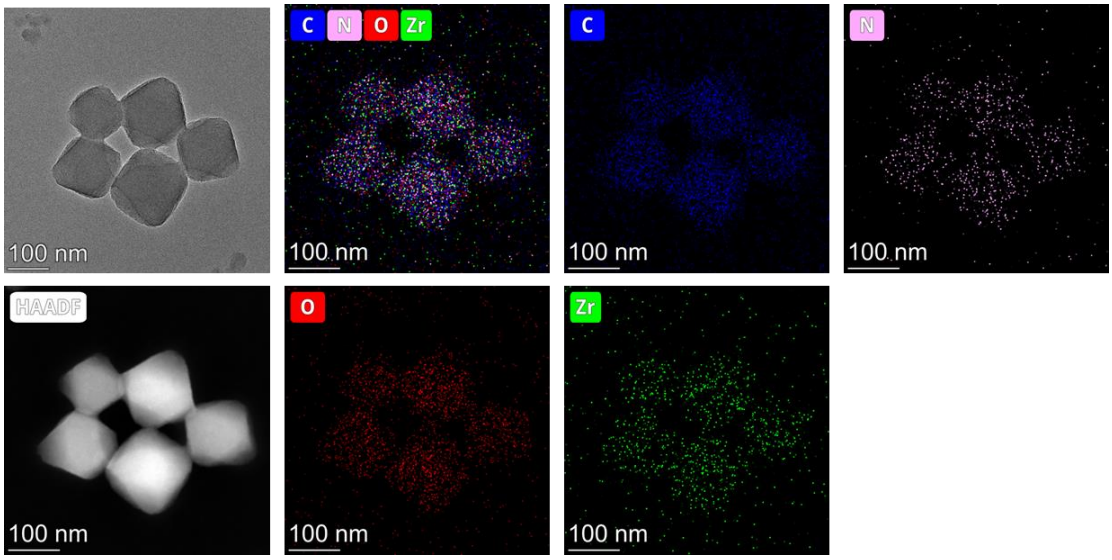

Fig. S14. TEM images and elemental mapping of PCN-160-4.

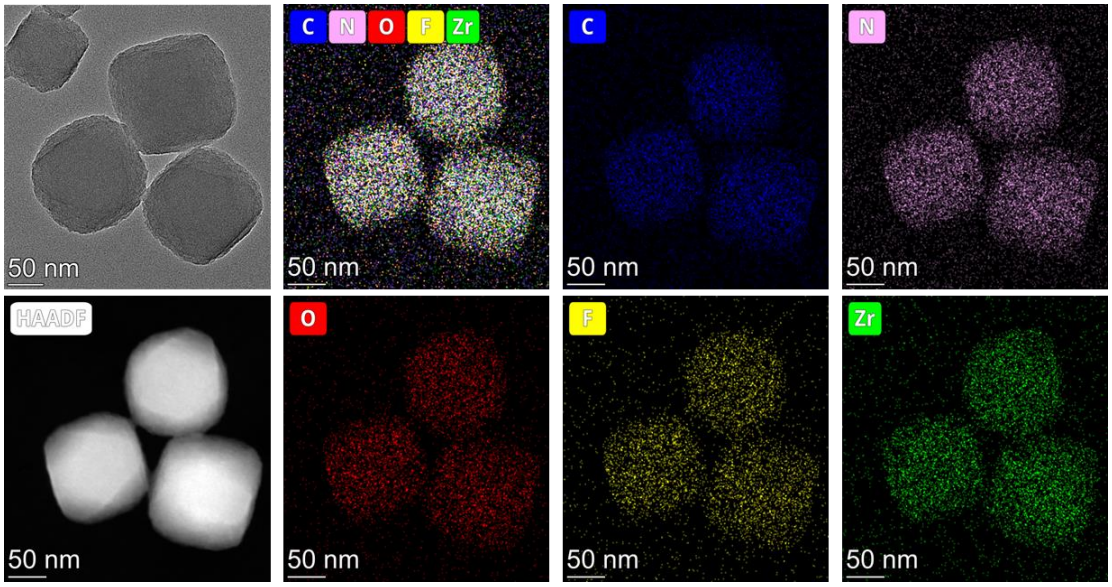

Fig. S15. TEM images and elemental mapping of PCN-160-5.

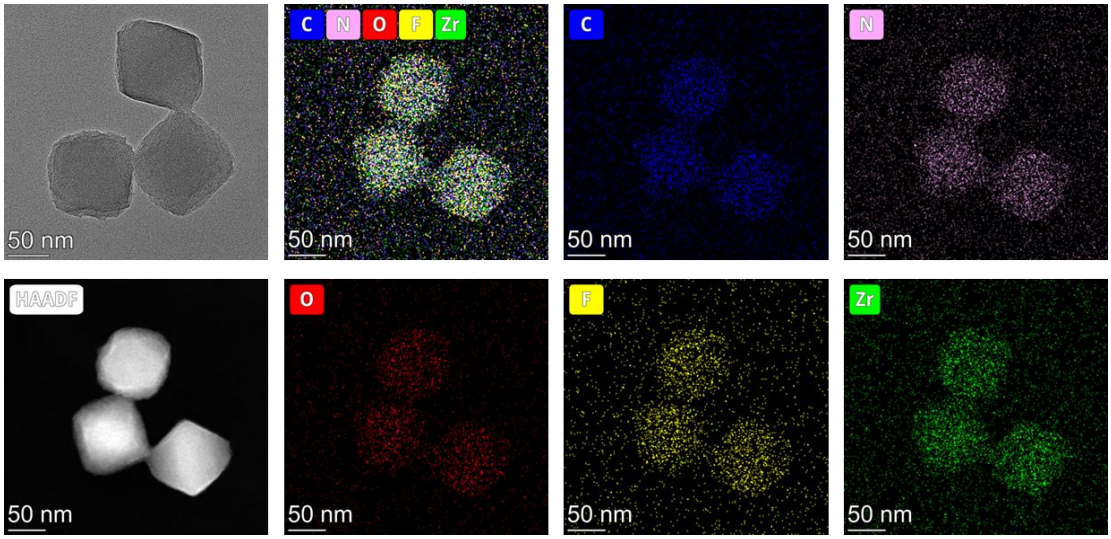

Fig. S16. TEM images and elemental mapping of PCN-160-7.

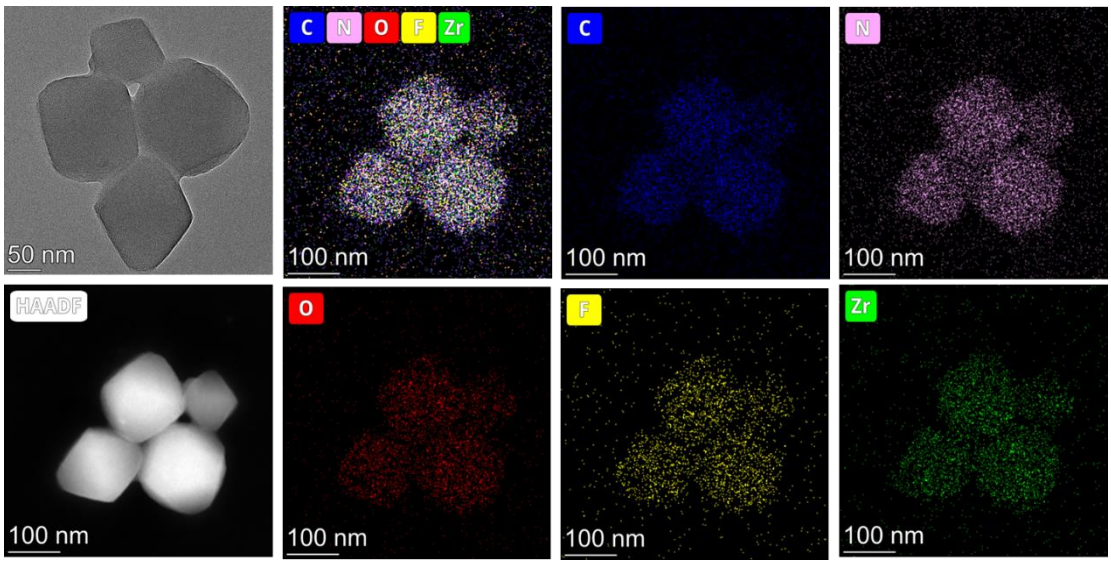

Fig. S17. TEM images and elemental mapping of PCN-160-9.

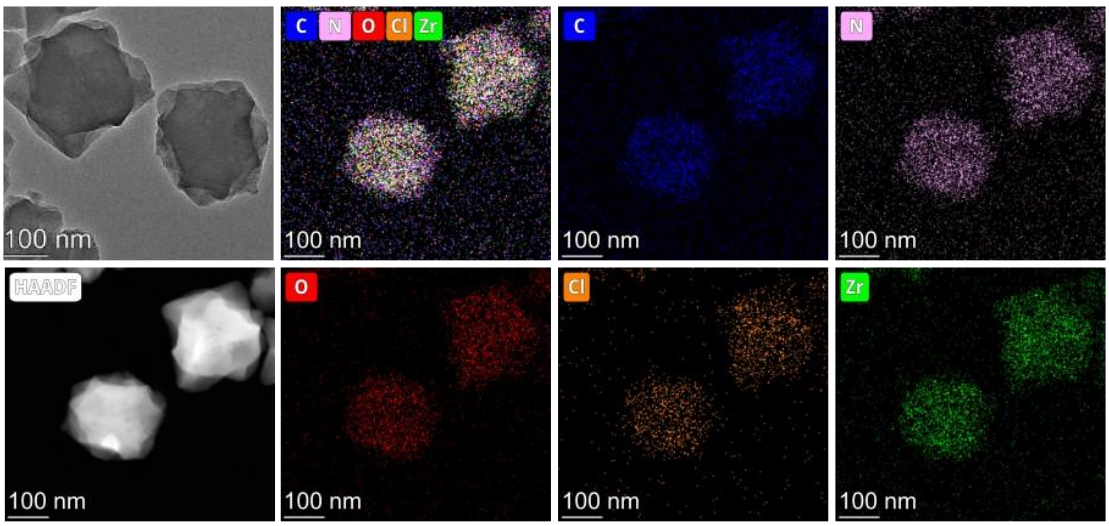

Fig. S18. TEM images and elemental mapping of PCN-160-10.

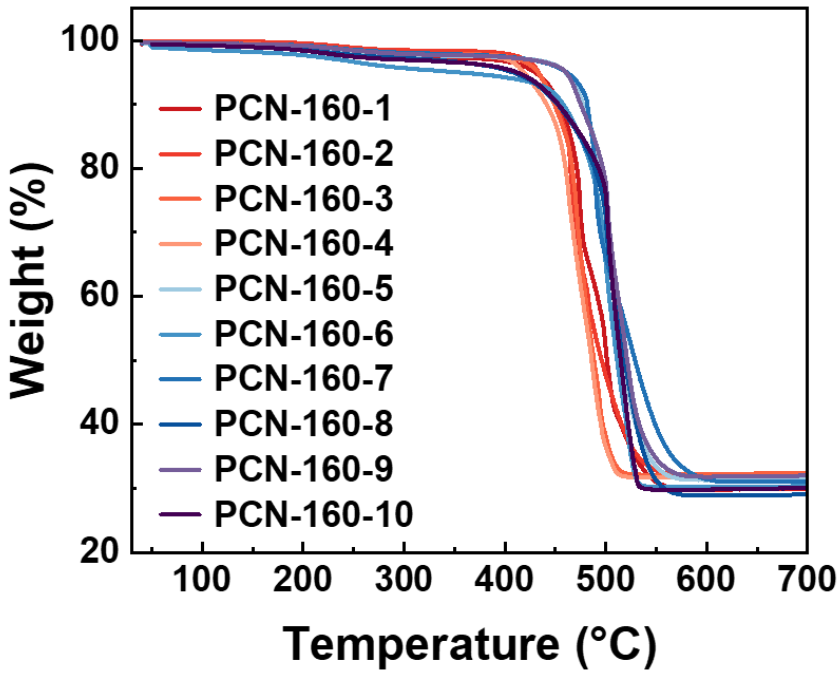

Fig. S19. TGA curve of PCN-160-X (X = 1-10).

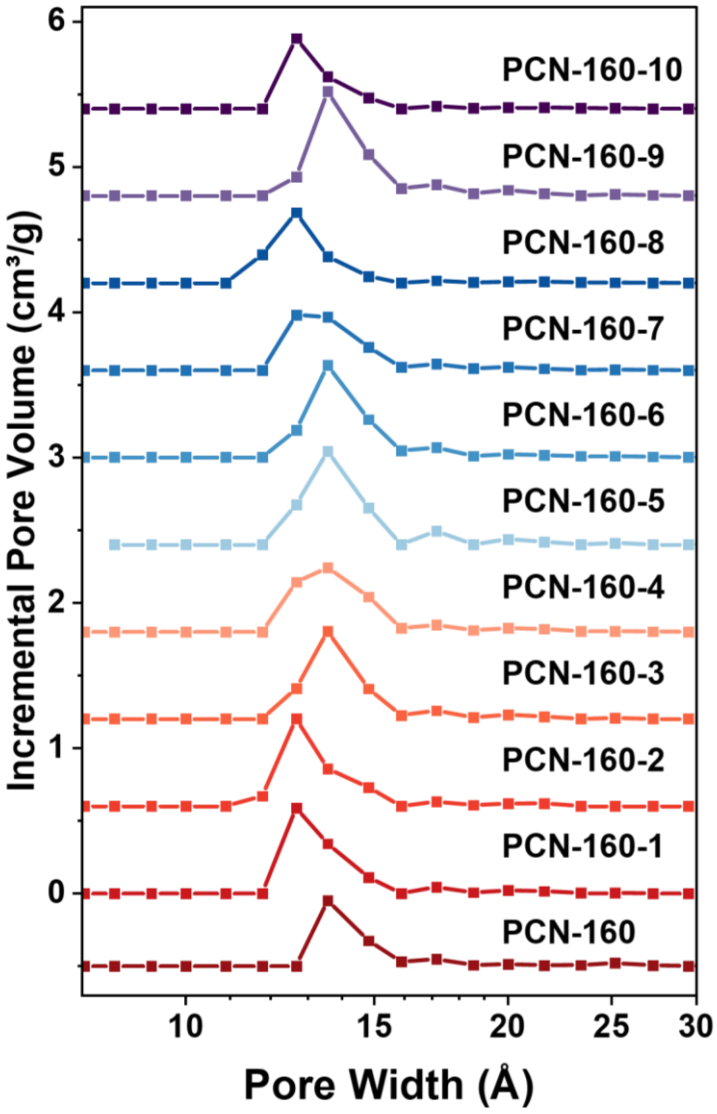

Fig. S20. Pore size distribution of PCN-160-X (X = 1-10).

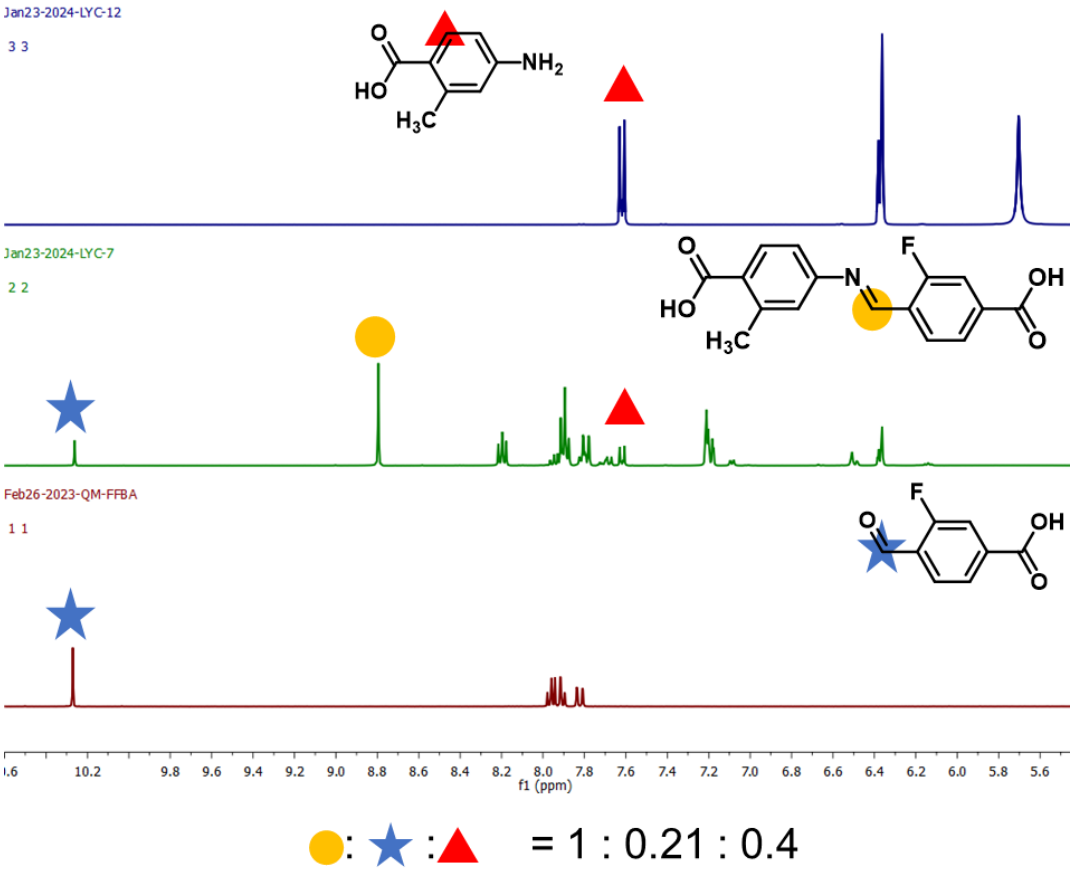

Fig. S21. ^{1}H NMR analysis of the formation of imine bonds between 4-amino-2-methylbenzoic acid and 3-fluoro-4-formylbenzoic acid.

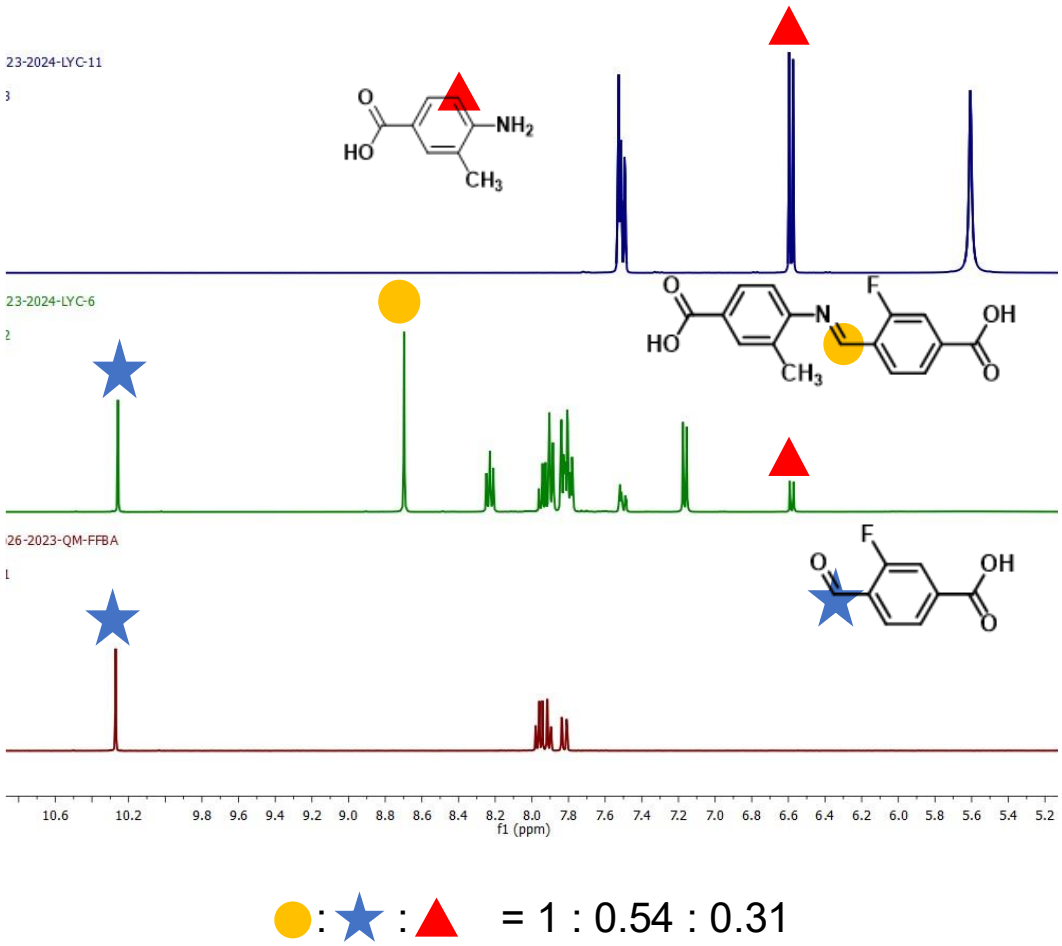

Fig. S22. ^{1}H NMR analysis of the formation of imine bonds between 4-amino-3-methylbenzoic acid and 3-fluoro-4-formylbenzoic acid.

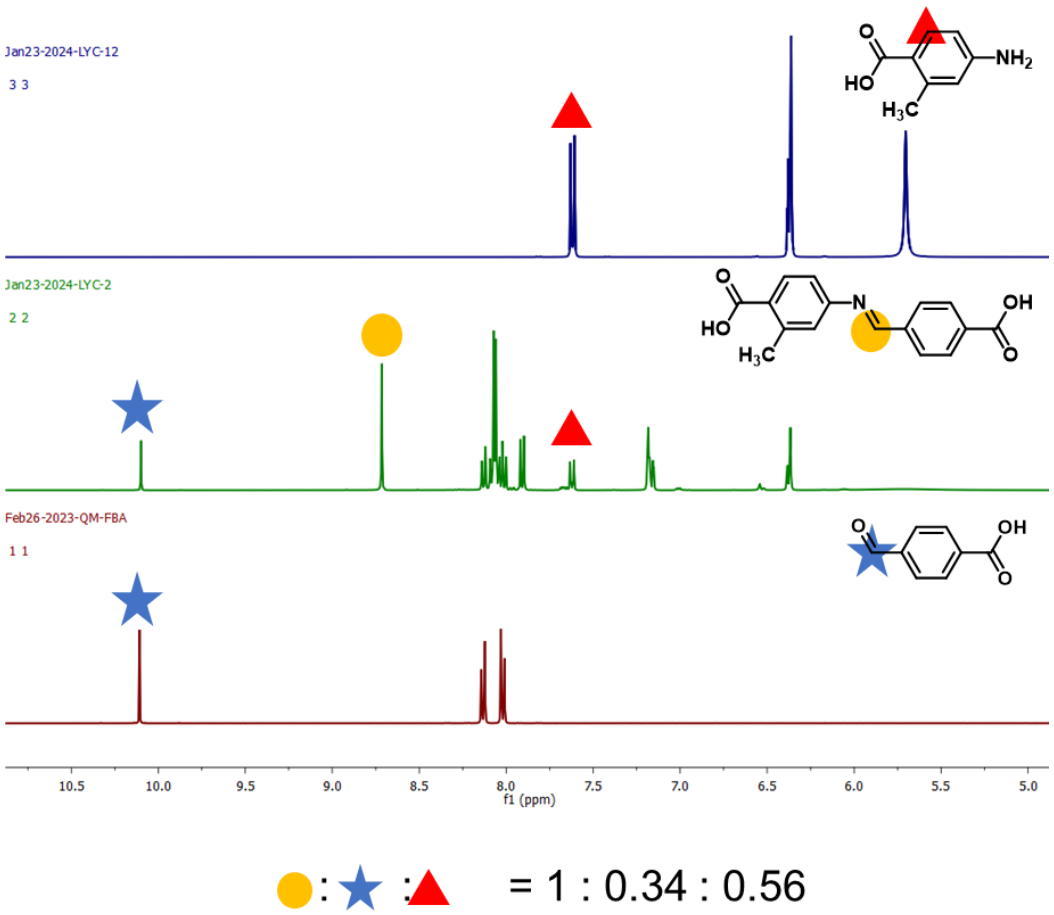

Fig. S23. ^{1}H NMR analysis of the formation of imine bonds between 4-amino-2-methylbenzoic acid and 4-formylbenzoic acid.

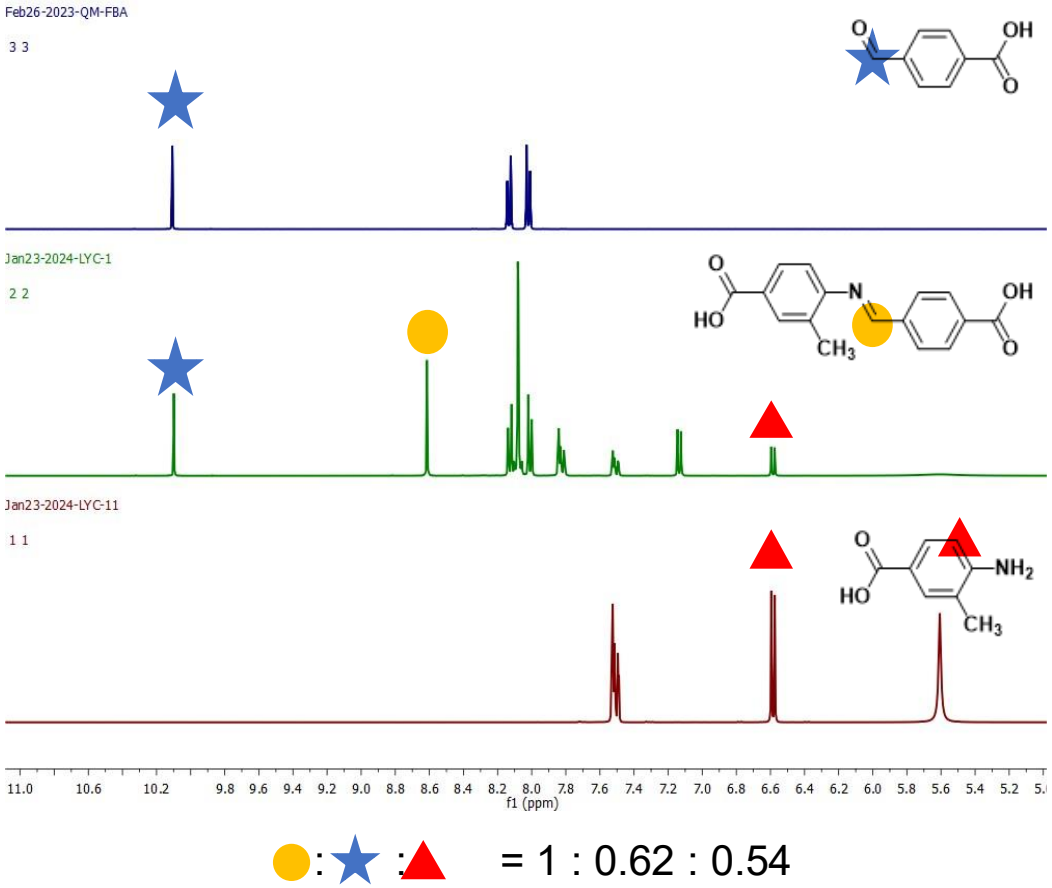

Fig. S24. ^{1}H NMR analysis of the formation of imine bonds between 4-amino-3-methylbenzoic acid and 4-formylbenzoic acid.

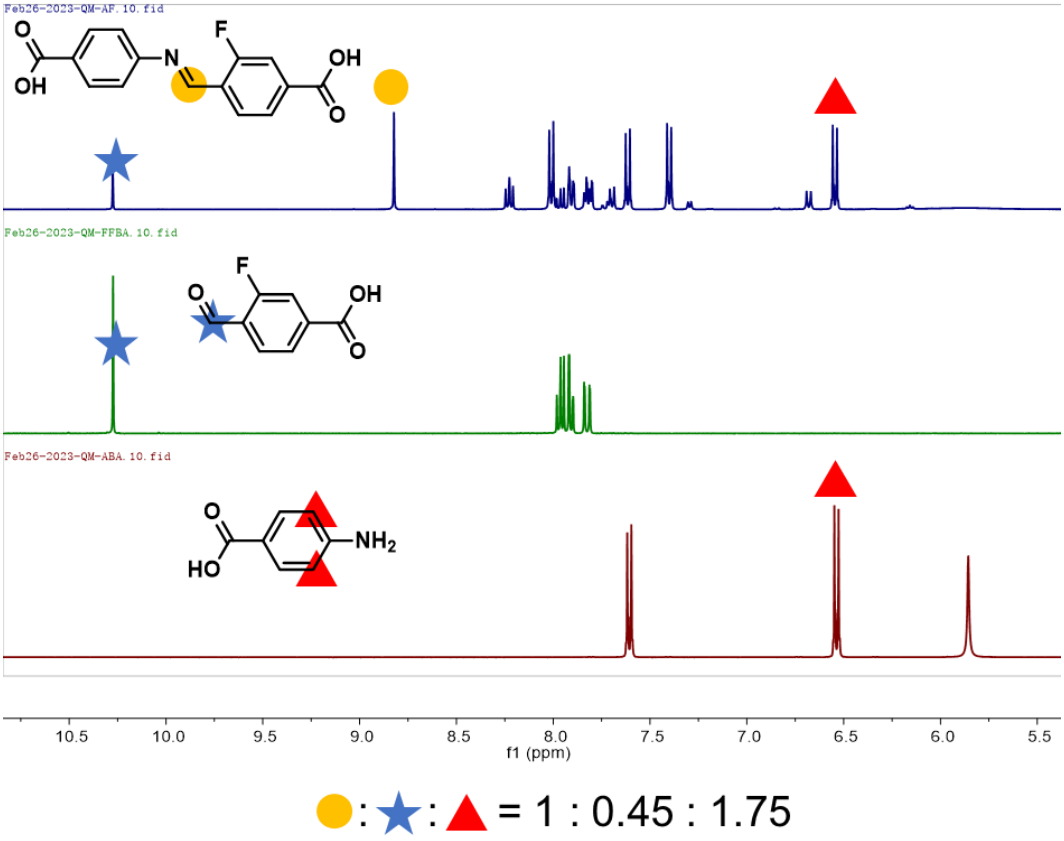

Fig. S25. ^{1}H NMR analysis of the formation of imine bonds between 4-aminobenzoic acid and 3-fluoro-4-formylbenzoic acid.

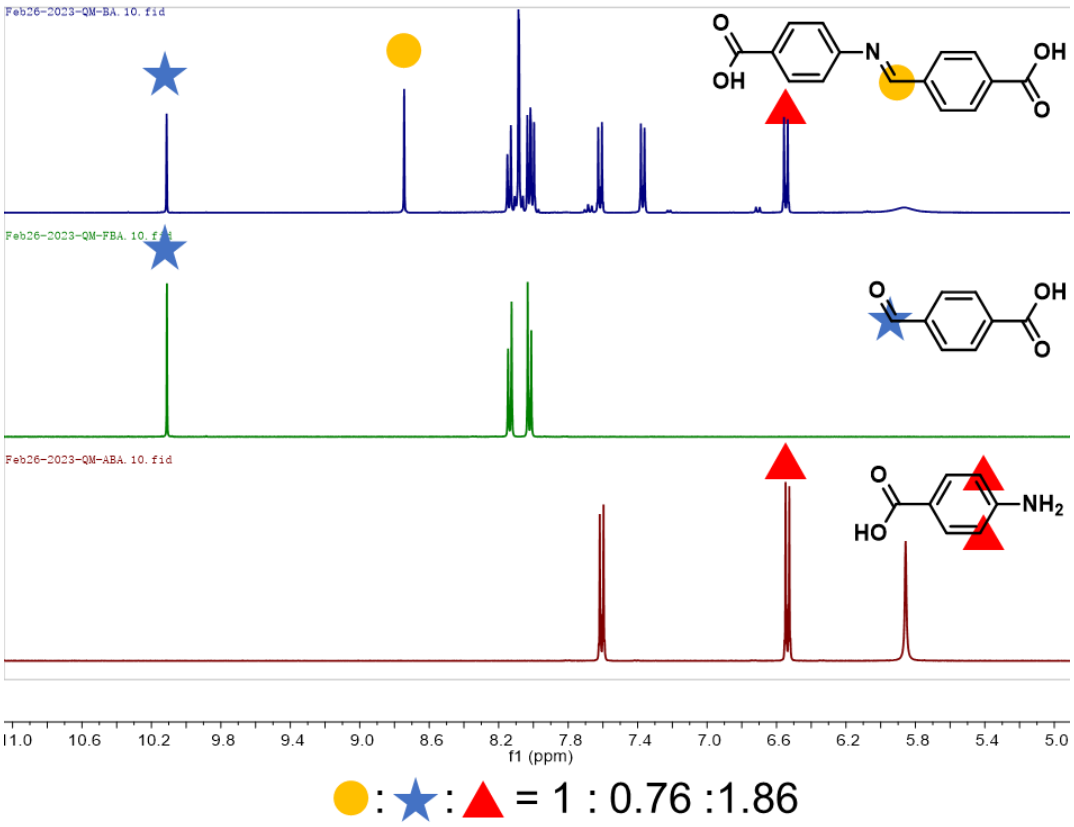

Fig. S26. ^{1}H NMR analysis of the formation of imine bonds between 4-aminobenzoic acid and 4-formylbenzoic acid.

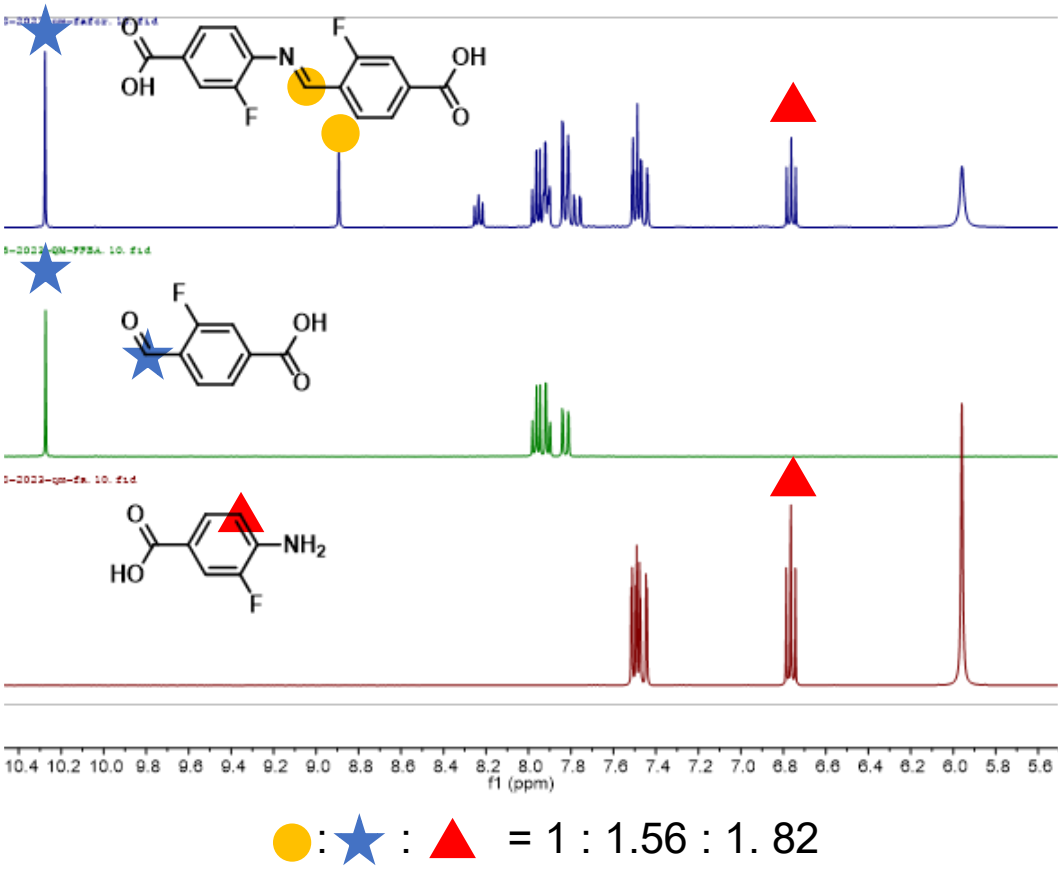

Fig. S27. ^{1}H NMR analysis of the formation of imine bonds between 4-amino-3-fluorobenzoic acid and 3-fluoro-4-formylbenzoic acid.

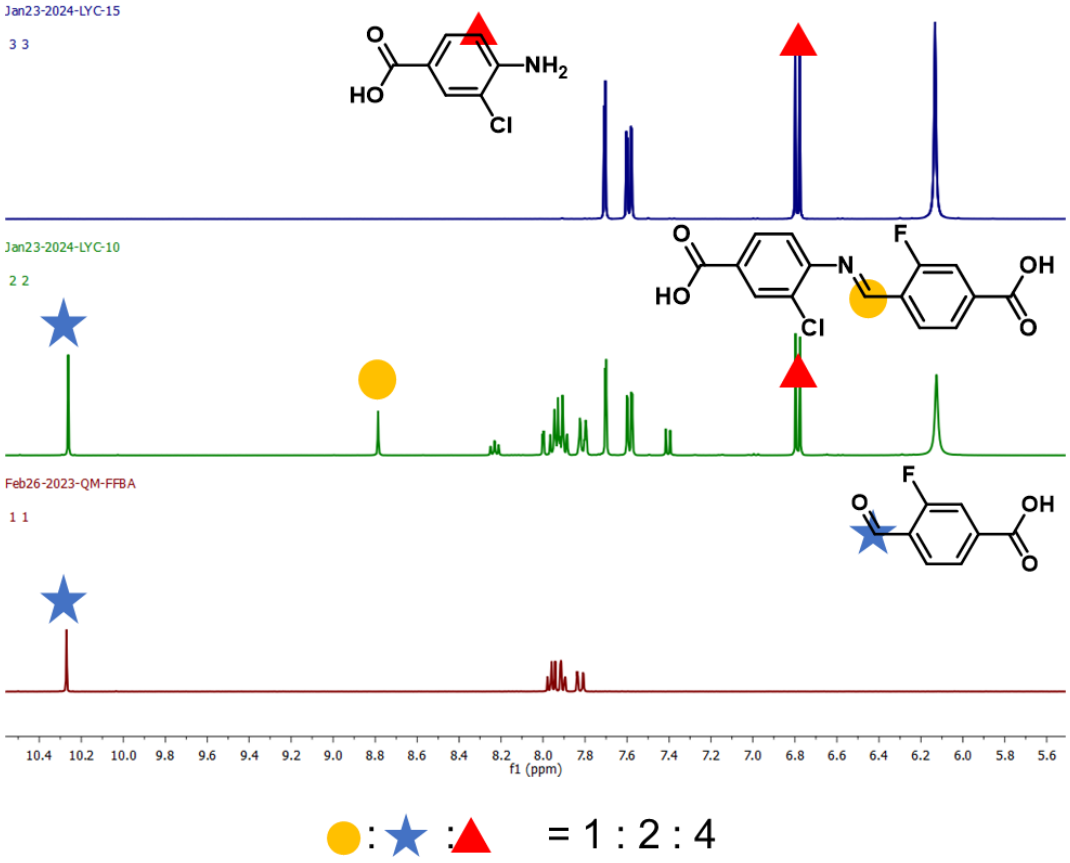

Fig. S28. ^{1}H NMR analysis of the formation of imine bonds between 4-amino-3-chlorobenzoic acid and 3-fluoro-4-formylbenzoic acid.

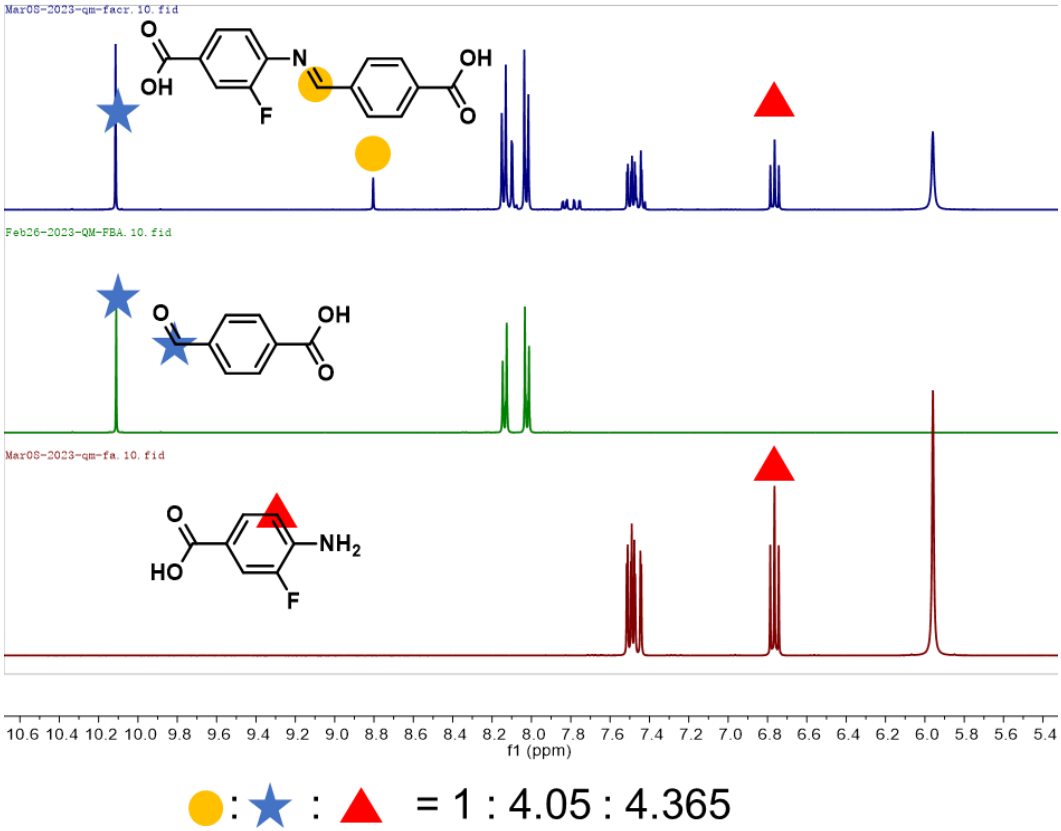

Fig. S29. ^{1}H NMR analysis of the formation of imine bonds between 4-amino-3-fluorobenzoic acid and 4-formylbenzoic acid.

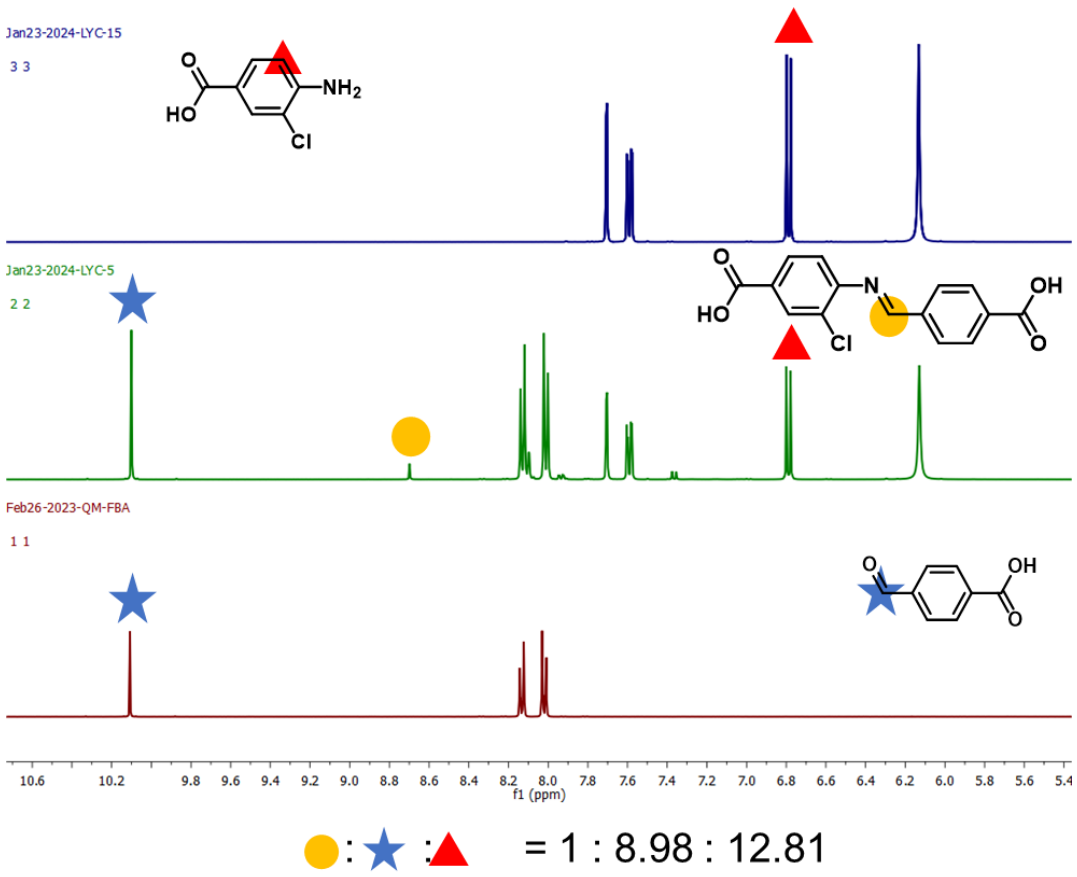

Fig. S30. ^{1}H NMR analysis of the formation of imine bonds between 4-amino-3-chlorobenzoic acid and 4-formylbenzoic acid.

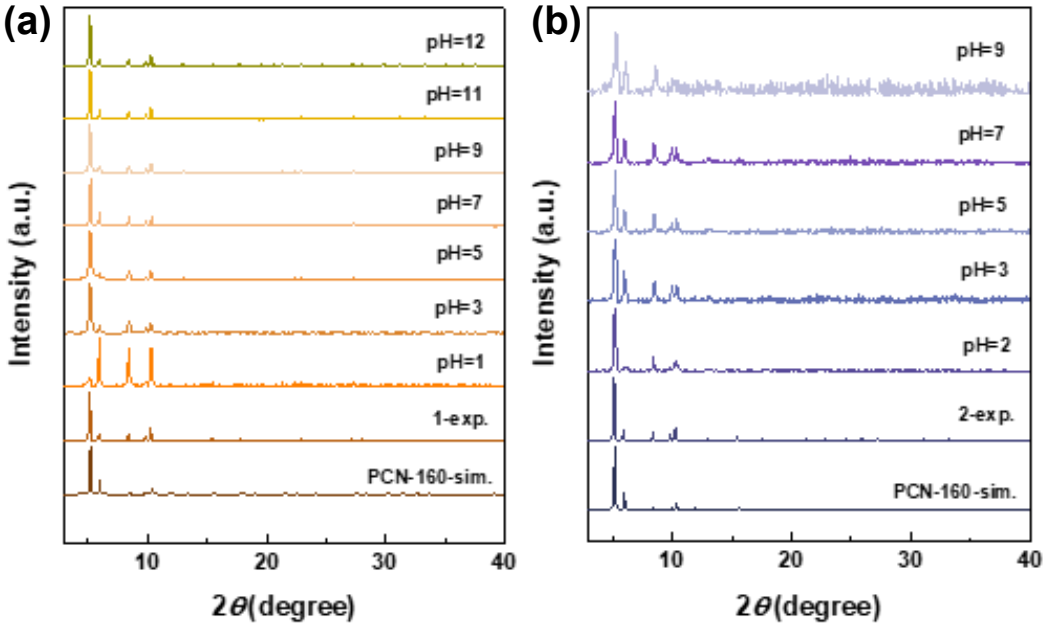

Fig. S31. PXRD patterns of PCN-160-1 (a) and PCN-160-2 (b) after incubation in aqueous solutions at various pH values.

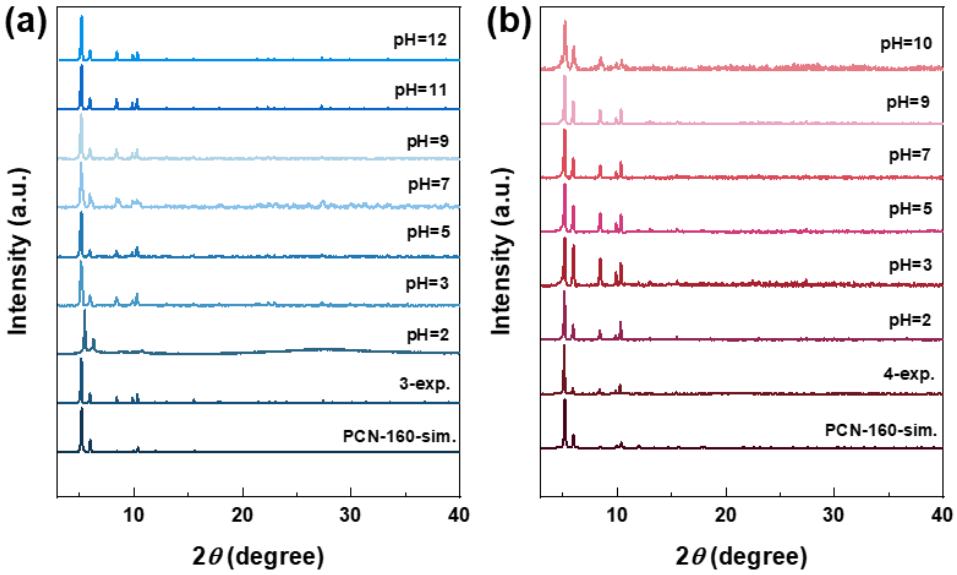

Fig. S32. PXRD patterns of PCN-160-3 (a) and PCN-160-4 (b) after incubation in aqueous solutions at various pH values.

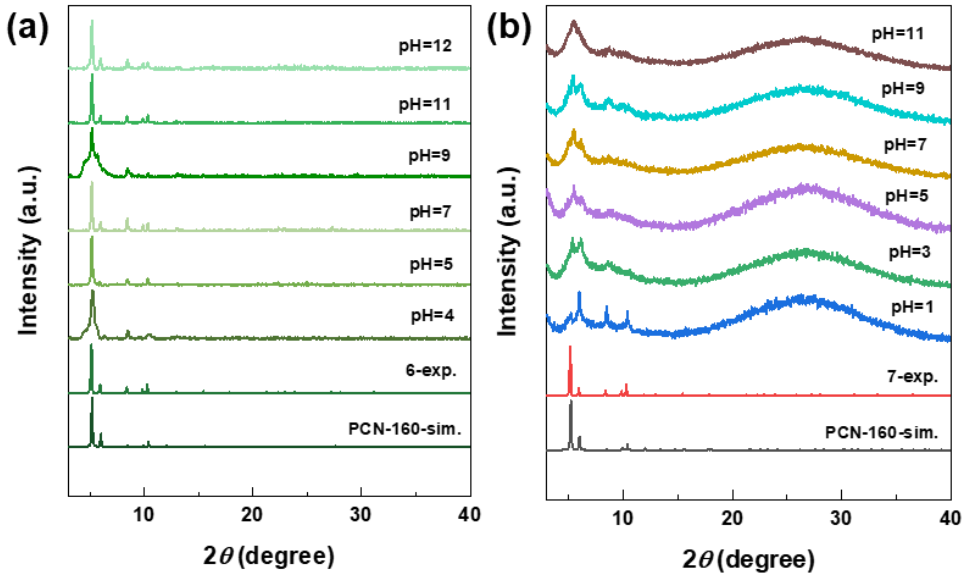

Fig. S33. PXRD patterns of PCN-160-6 (a) and PCN-160-7 (b) after incubation in aqueous solutions at various pH values.

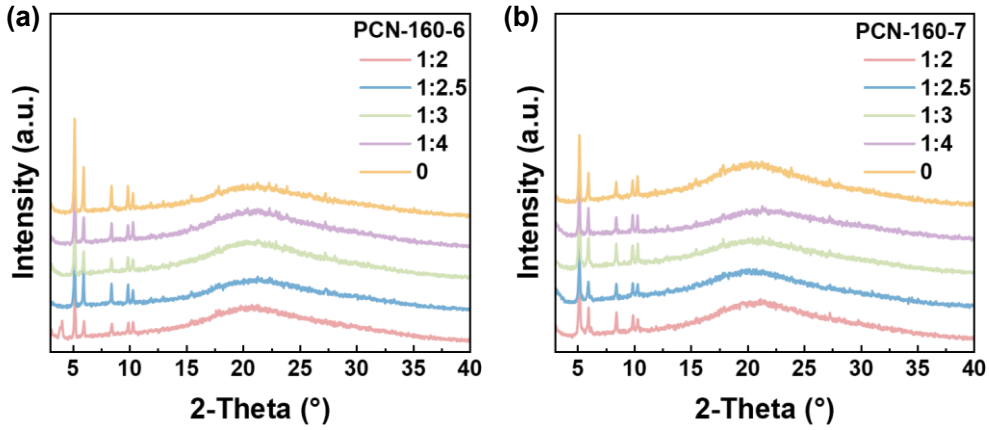

Fig. S34. PXRD patterns of PCN-160-6 (a) and PCN-160-7 (b) after incubation in H_2O/DMSO mixtures with varying volume ratios.

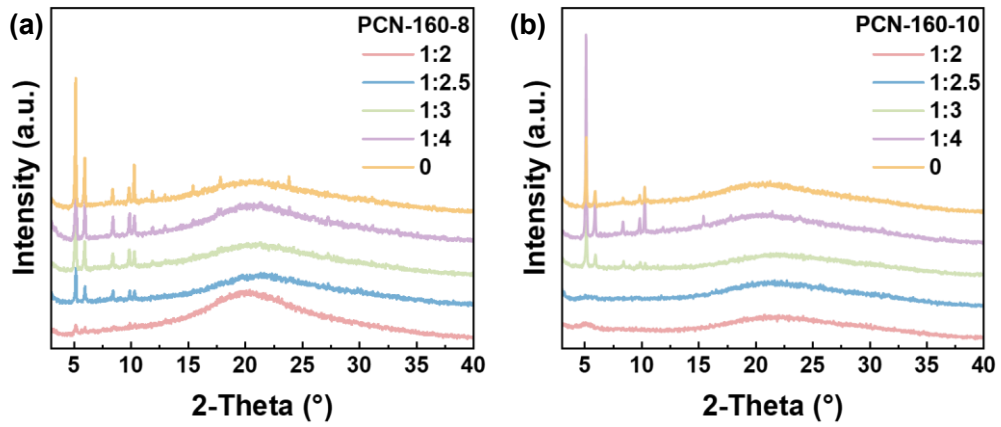

Fig. S35. PXRD patterns of PCN-160-8 (a) and PCN-160-10 (b) after incubation in H_2O/DMSO mixtures with varying volume ratios.

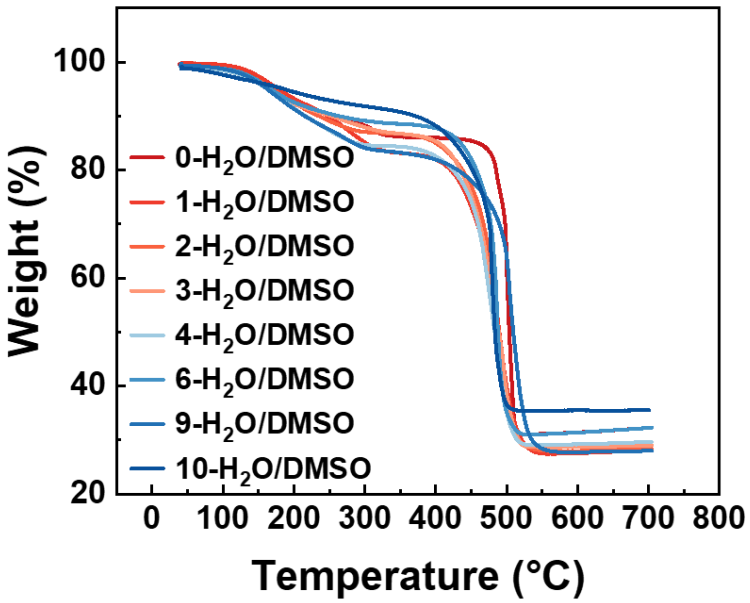

Fig. S36. TGA curve of PCN-160-X (X = 1-10) after treatment in H_2O/DMSO (1:2 v/v).

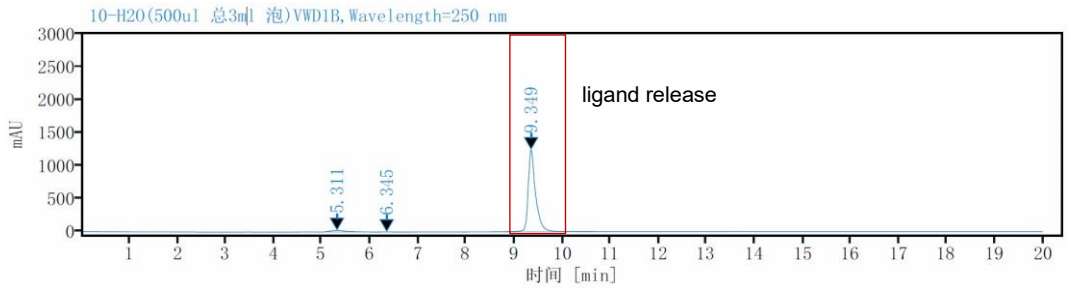

Fig. S37. HPLC analysis of ligand release from PCN-160-10 following aqueous incubation.

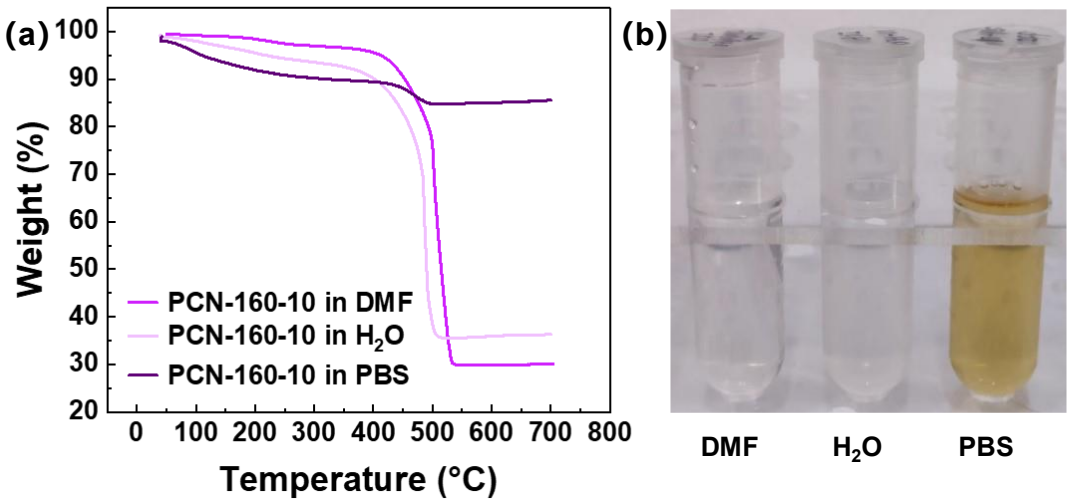

Fig. S38. (a) TGA curve of PCN-160-10 after the treatment by H_2O and PBS. (b) Photographs of supernatants obtained after centrifuging PCN-160-10 treated with DMF, water, and PBS. The water-treated sample shows a colorless supernatant consistent with minimal ligand leaching. In contrast, the PBS-treated sample exhibits a distinct yellow color, indicating framework disintegration and significant ligand release.

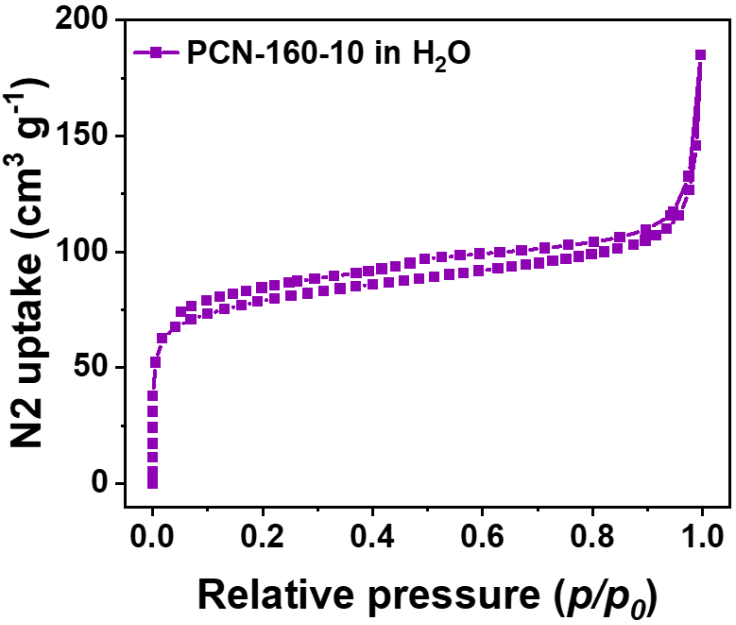

Fig. S39. N_2 absorption-desorption isotherms of PCN-160-10 after 12 h of aqueous incubation.

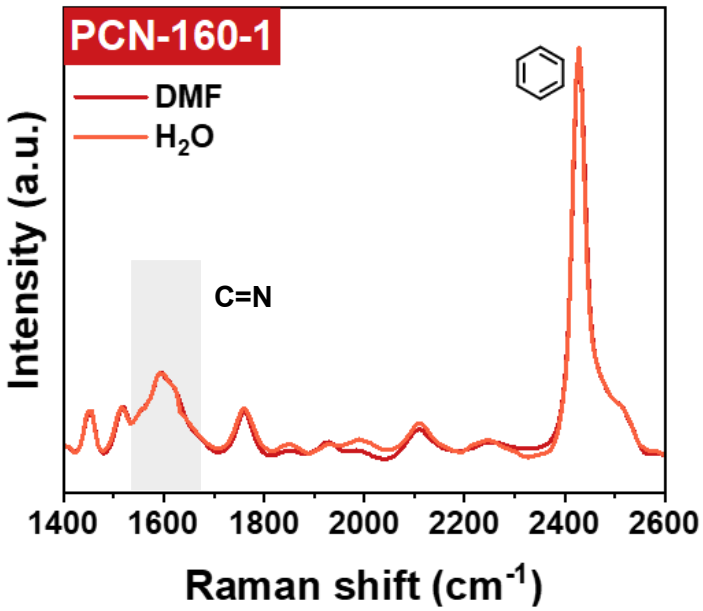

Fig. S40. Raman spectra of PCN-160-1 under different conditions: prepared in DMF and immersed in H_2O.

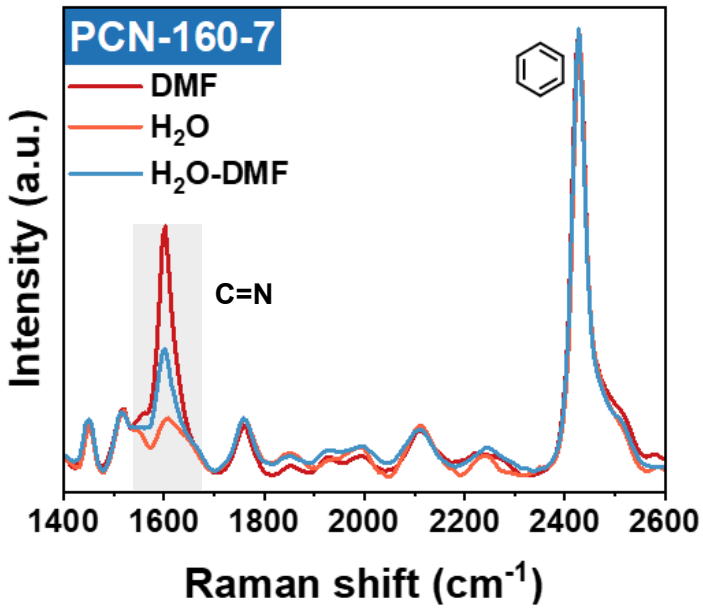

Fig. S41. Raman spectra of PCN-160-7 under different conditions (as-synthesized in DMF, after water immersion, and redissolved in DMF), revealing reversible and irreversible imine bond behavior.

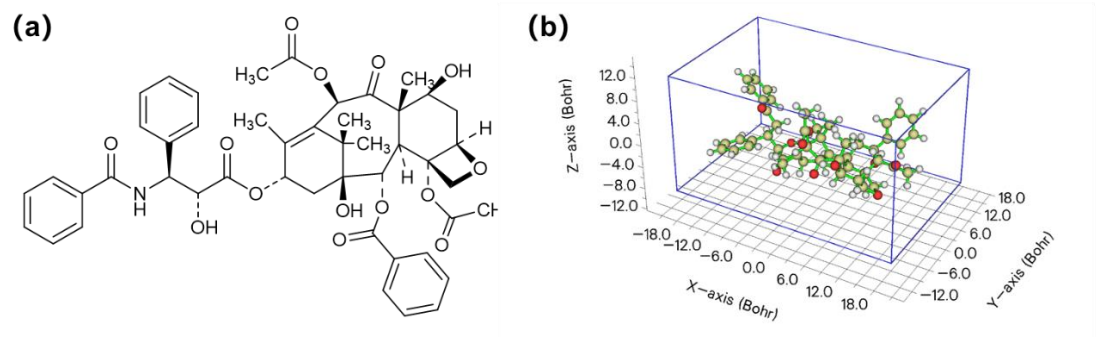

Fig. S42. The structure (a) and size analysis (b) of paclitaxel by Multiwfn. Paclitaxel: 20.880×13.510×11.195 Å.

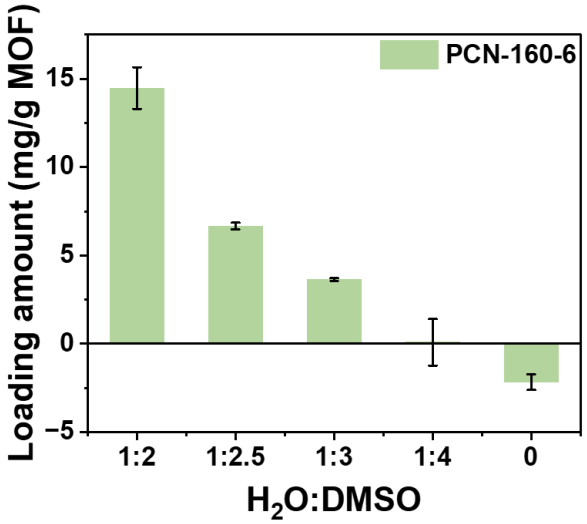

Fig. S43. Effect of H_2O/DMSO volume ratios on the paclitaxel adsorption capacity of PCN-160-6.

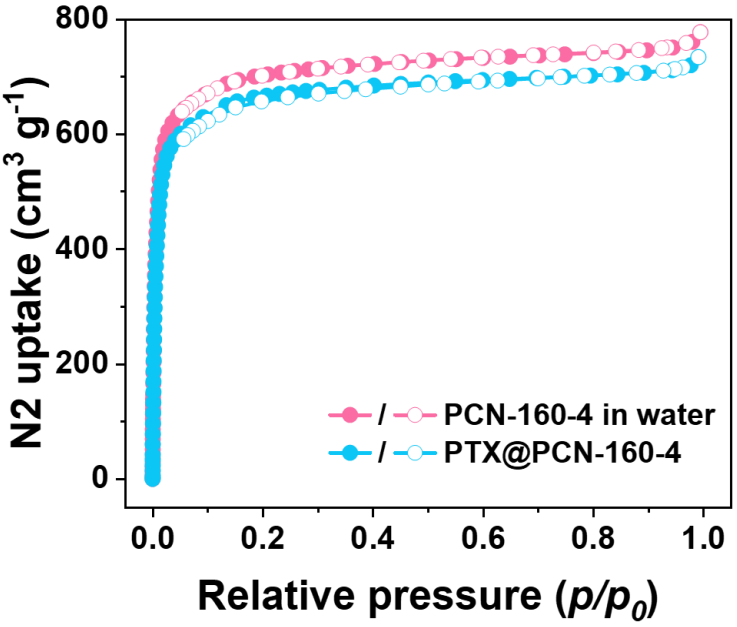

Fig. S44. N_2 sorption of PCN-160-4 after aqueous incubation and PTX loading, confirming preserved porosity.

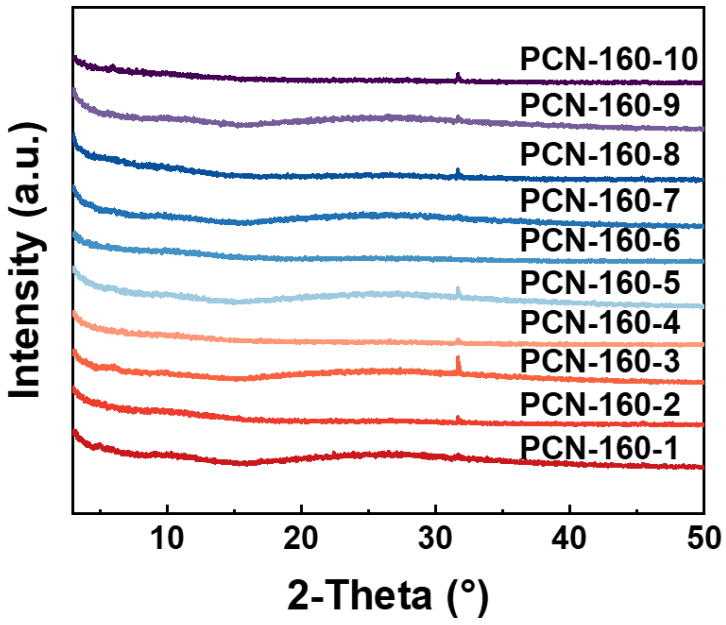

Fig. S45. PXRD of PCN-160-X (X = 1-10) incubated in PBS.

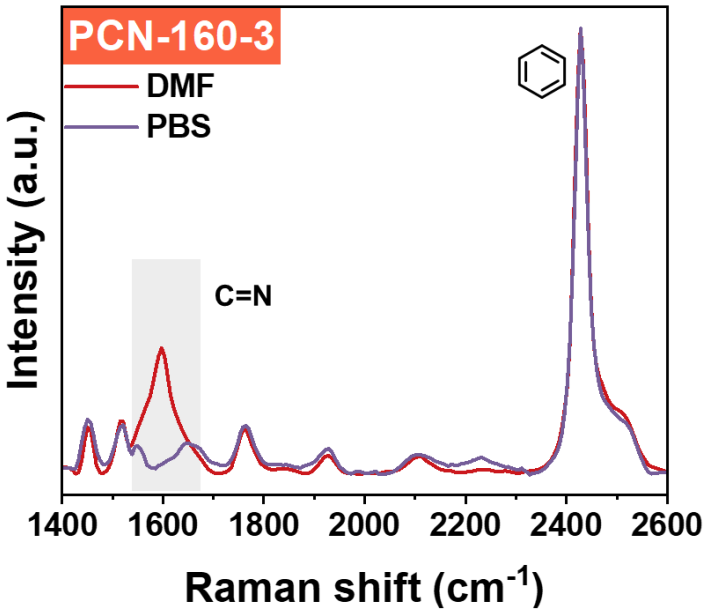

Fig. S46. Raman spectra of PCN-160-3 under different conditions (as-synthesized in DMF, and in PBS).

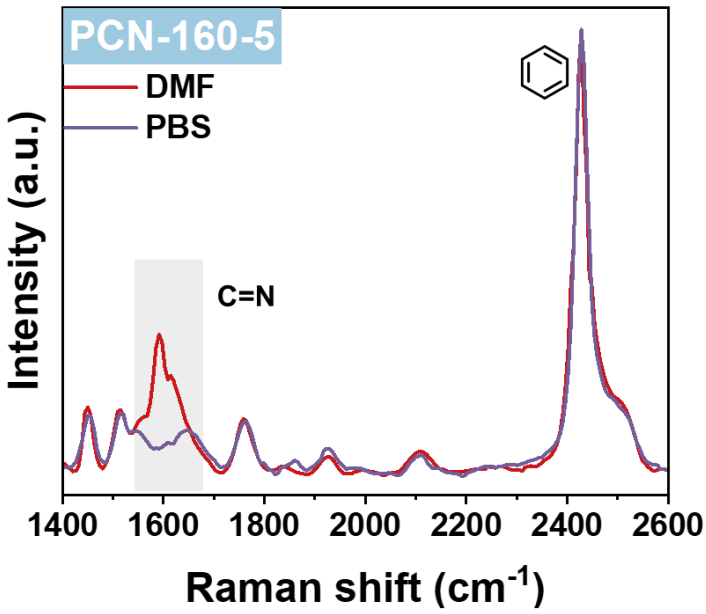

Fig. S47. Raman spectra of PCN-160-5 under different conditions (as-synthesized in DMF, and in PBS).

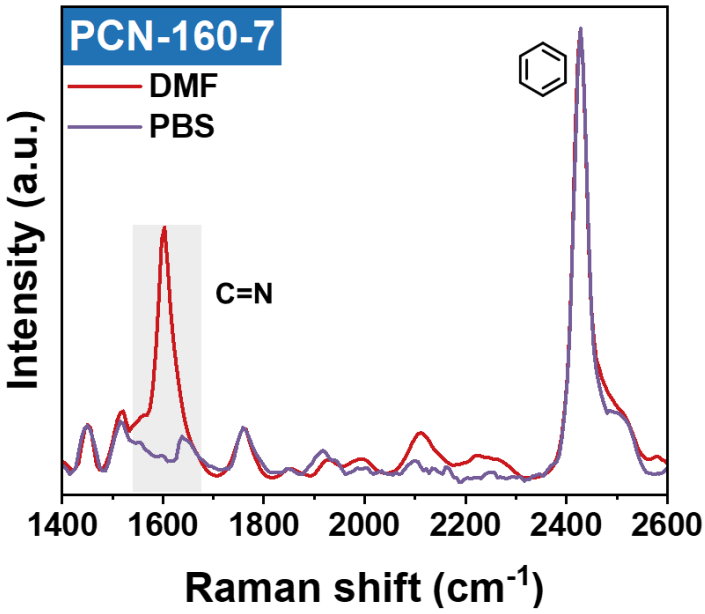

Fig. S48. Raman spectra of PCN-160-7 under different conditions (as-synthesized in DMF, and in PBS).

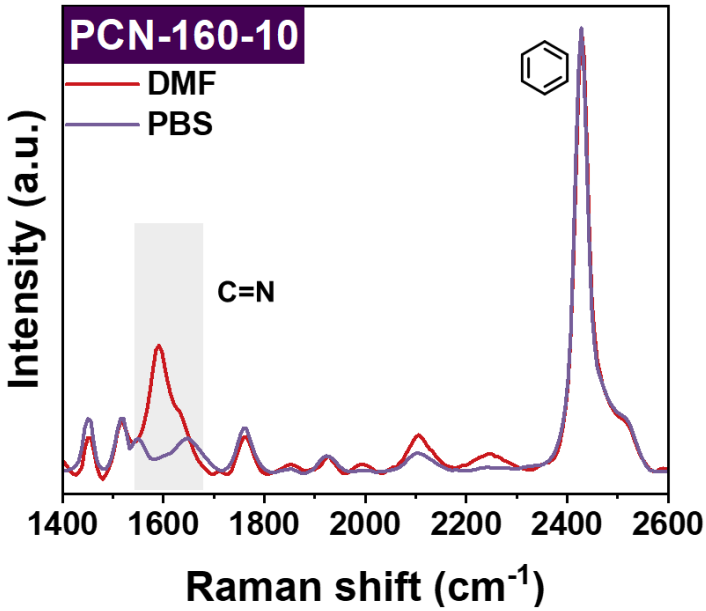

Fig. S49. Raman spectra of PCN-160-10 under different conditions (as-synthesized in DMF, and in PBS).

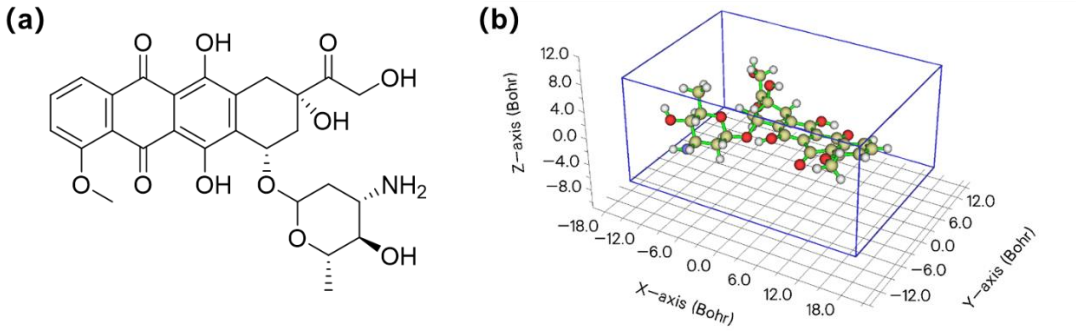

Fig. S50. The structure (a) and size analysis (b) of epirubicin by Multiwfn. Epirubicin: 18.211×12.658×8.36 Å.

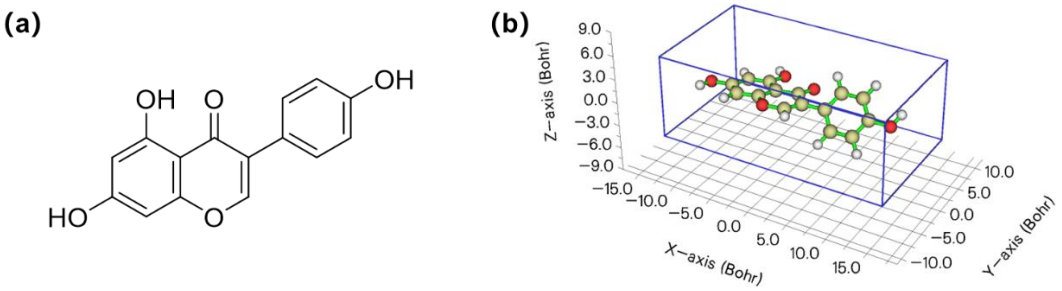

Fig. S51. The structure (a) and size analysis (b) of genistein by Multiwfn. Genistein: 15.106×8.237×5.605 Å.

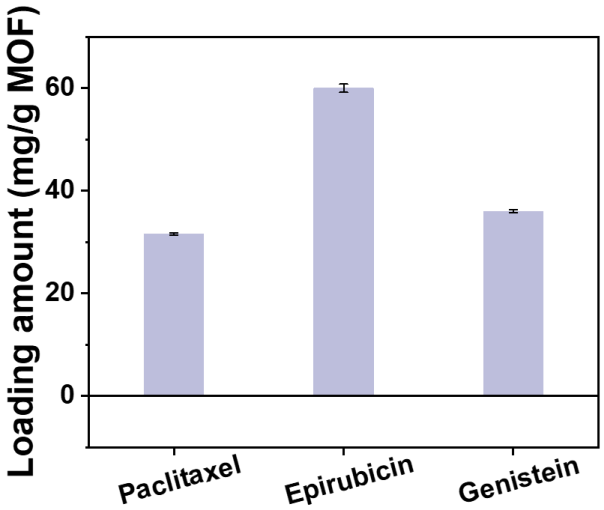

Fig. S52. The loading of therapeutic drugs by PCN-160-4.

Table Section

Tab. S1. Preparation of the exchange solution for PCN-160-X.

Entry	Reagent 1 (0.5 mol)	Reagent 2 (0.5 mol)	Solvent
1	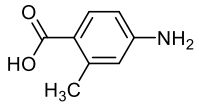	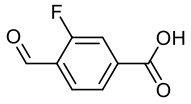	
	4-Amino-2-methylbenzoic acid	3-Fluoro-4-formylbenzoic acid	
2	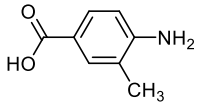	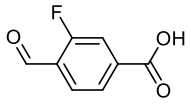	
	4-Amino-3-methylbenzoic acid	3-Fluoro-4-formylbenzoic acid	
3	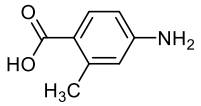	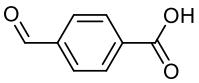	
	4-Amino-2-methylbenzoic acid	4-Formylbenzoic acid	
4	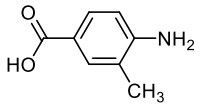	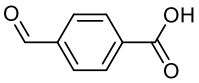	
	4-Amino-3-methylbenzoic acid	4-Formylbenzoic acid	
5	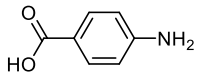	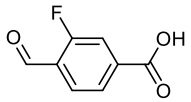	
	4-Aminobenzoic acid	3-Fluoro-4-formylbenzoic acid	DMF (50 mL)
6	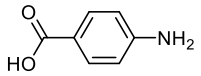	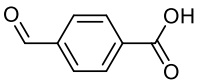	
	4-Aminobenzoic acid	4-Formylbenzoic acid	
7	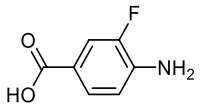	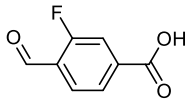	
	4-Amino-3-fluorobenzoic acid	3-Fluoro-4-formylbenzoic acid	
8	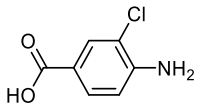	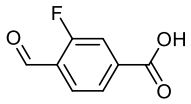	
	4-Amino-3-chlorobenzoic acid	3-Fluoro-4-formylbenzoic acid	
9	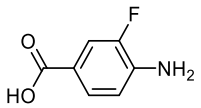	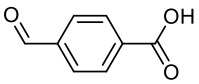	
	4-Amino-3-fluorobenzoic acid	4-Formylbenzoic acid	
10	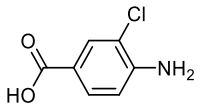	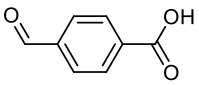	
	4-Amino-3-chlorobenzoic acid	4-Formylbenzoic acid	

Tab. S2. Crystal data and structure refinement parameters of PCN-160-1, PCN-160-2, and PCN-160-3.

Name	PCN-160-1	PCN-160-2	PCN-160-3
CCDC	2538817	2538819	2538816
Empirical formula	$C_{96}H_{60}F_6N_6O_{32}Zr_6$	$C_{96}H_{60}F_6N_6O_{32}Zr_6$	$C_{96}H_{66}N_6O_{32}Zr_6$
Formula weight	2470.82	2470.82	2362.86
Temperature/K	193	193	193
Crystal system	cubic	cubic	cubic
Space group	*Fm-3m*	*Fm-3m*	*Fm-3m*
a/Å	29.5473(18)	29.4901(17)	29.6733(16)
b/Å	29.5473(18)	29.4901(17)	29.6733(16)
c/Å	29.5473(18)	29.4901(17)	29.6733(16)
α/°	90	90	90
β/°	90	90	90
γ/°	90	90	90
V/Å^3	25796(5)	25647(4)	26127(4)
Z	4	4	4
ρ_{calc}/gcm^{-3}	0.637	0.640	0.601
μ/mm^{-1}	0.270	0.272	0.262
F(000)	4912.0	4912.0	4720.0
Crystal size/mm^3	0.13 × 0.12 × 0.1	0.13 × 0.12 × 0.1	0.13 × 0.12 × 0.1
Radiation	MoK_α (λ = 0.71073)	MoK_α (λ = 0.71073)	MoK_α (λ = 0.71073)
2Θ range for data collection/°	4.776 to 49.418	3.906 to 49.412	3.882 to 49.368
Index ranges	-34 ≤ *h* ≤ 34, -34 ≤ *k* ≤ 34, -34 ≤ *l* ≤ 32	-33 ≤ *h* ≤ 34, -34 ≤ *k* ≤ 34, -34 ≤ *l* ≤ 34	-34 ≤ *h* ≤ 34, -34 ≤ *k* ≤ 34, -34 ≤ *l* ≤ 34
Reflections collected	35601	36500	40193
Independent reflections	1149 [R_{int} = 0.1345, R_{sigma} = 0.0337]	1152 [R_{int} = 0.1041, R_{sigma} = 0.0285]	1161 [R_{int} = 0.0634, R_{sigma} = 0.0160]
Data/restraints/parameters	1149/132/108	1152/137/110	1161/129/93
Goodness-of-fit on F^2	1.085	1.260	1.257
Final *R* indexes [*I*>=2σ(*I*)][a,b]	R_1 = 0.0818, wR_2 = 0.2360	R_1 = 0.0955, wR_2 = 0.2784	R_1 = 0.0453, wR_2 = 0.1372
Final *R* indexes [all data][a,b]	R_1 = 0.0978, wR_2 = 0.2610	R_1 = 0.1067, wR_2 = 0.2968	R_1 = 0.0479, wR_2 = 0.1413
Largest diff. peak/hole / e Å^{-3}	1.35/-0.84	1.12/-0.48	1.00/-0.36

[a] $R_1 = \Sigma||F_o| - |F_c||/\Sigma|F_o|$.

[b] $wR_2 = |\Sigma w(|F_o|^2 - |F_c|^2)|/\Sigma|w(F_o^2)^2|^{1/2}$.

Tab. S3. Crystal data and structure refinement parameters of PCN-160-4, PCN-160-5, and PCN-160-7.

Name	PCN-160-4	PCN-160-5	PCN-160-7
CCDC	2538822	2538815	2538818
Empirical formula	$C_{96}H_{66}N_6O_{32}Zr_6$	$C_{90}H_{48}F_6N_6O_{32}Zr_6$	$C_{90}H_{42}F_{12}N_6O_{32}Zr_6$
Formula weight	2362.86	2386.66	2494.61
Temperature/K	193	193	193
Crystal system	cubic	cubic	cubic
Space group	*Fm-3m*	*Fm-3m*	*Fm-3m*
a/Å	29.615(6)	29.5094(19)	29.659(2)
b/Å	29.615(6)	29.5094(19)	29.659(2)
c/Å	29.615(6)	29.5094(19)	29.659(2)
α/°	90	90	90
β/°	90	90	90
γ/°	90	90	90
V/Å^3	25973(14)	25697(5)	26089(5)
Z	4	4	4
ρ_{calc}/gcm^{-3}	0.604	0.617	0.635
μ/mm^{-1}	0.264	0.270	0.271
F(000)	4720.0	4720.0	4912.0
Crystal size/mm^3	0.13 × 0.12 × 0.1	0.13 × 0.12 × 0.1	0.13 × 0.12 × 0.1
Radiation	MoK_α (λ = 0.71073)	MoK_α (λ = 0.71073)	MoK_α (λ = 0.71073)
2Θ range for data collection/°	3.89 to 49.364	3.904 to 49.398	3.884 to 49.394
Index ranges	-34 ≤ *h* ≤ 34, -34 ≤ *k* ≤ 34, -34 ≤ *l* ≤ 33	-34 ≤ *h* ≤ 34, -34 ≤ *k* ≤ 34, -34 ≤ *l* ≤ 32	-34 ≤ *h* ≤ 34, -34 ≤ *k* ≤ 34, -34 ≤ *l* ≤ 33
Reflections collected	35952	35678	36035
Independent reflections	1163 [R_{int} = 0.1309, R_{sigma} = 0.0333]	1153 [R_{int} = 0.1301, R_{sigma} = 0.0332]	1165 [R_{int} = 0.1309, R_{sigma} = 0.0333]
Data/restraints/parameters	1163/111/94	1153/105/94	1165/105/94
Goodness-of-fit on F^2	1.075	1.088	1.126
Final *R* indexes [*I*>=2σ(*I*)][a,b]	R_1 = 0.0822, wR_2 = 0.2432	R_1 = 0.0730, wR_2 = 0.2276	R_1 = 0.0834, wR_2 = 0.2589
Final *R* indexes [all data][a,b]	R_1 = 0.0978, wR_2 = 0.2705	R_1 = 0.0884, wR_2 = 0.2523	R_1 = 0.0987, wR_2 = 0.2852
Largest diff. peak/hole / e Å^{-3}	1.13/-0.49	0.90/-0.54	1.21/-0.46

[a] $R_1 = \Sigma||F_o| - |F_c||/\Sigma|F_o|$.

[b] $wR_2 = |\Sigma w(|F_o|^2 - |F_c|^2)|/\Sigma|w(F_o^2)^2|^{1/2}$.

Tab. S4. Crystal data and structure refinement parameters of PCN-160-8, PCN-160-9, and PCN-160-10.

Name	PCN-160-8	PCN-160-9	PCN-160-10
CCDC	2538820	2538821	2538814
Empirical formula	$C_{90}H_{42}Cl_6F_6N_6O_{32}Zr_6$	$C_{96}H_{48}F_6N_6O_{32}Zr_6$	$C_{90}H_{48}Cl_6N_6O_{32}Zr_6$
Formula weight	2593.31	2386.66	2485.36
Temperature/K	193	193	193
Crystal system	cubic	cubic	cubic
Space group	*Fm-3m*	*Fm-3m*	*Fm-3m*
a/Å	29.6519(11)	29.553(3)	29.5687(19)
b/Å	29.6519(11)	29.553(3)	29.5687(19)
c/Å	29.6519(11)	29.553(3)	29.5687(19)
α/°	90	90	90
β/°	90	90	90
γ/°	90	90	90
V/Å^3	26071(3)	25810(7)	25852(5)
Z	4	4	4
ρ_{calc}/gcm^{-3}	0.661	0.614	0.639
μ/mm^{-1}	0.329	0.269	0.327
F(000)	5104.0	4720.0	4912.0
Crystal size/mm^3	0.13 × 0.12 × 0.1	0.13 × 0.12 × 0.1	0.13 × 0.12 × 0.1
Radiation	MoK_α (λ = 0.71073)	MoK_α (λ = 0.71073)	MoK_α (λ = 0.71073)
2Θ range for data collection/°	3.886 to 49.406	3.898 to 49.408	4.568 to 49.38
Index ranges	-34 ≤ *h* ≤ 34, -34 ≤ *k* ≤ 34, -34 ≤ *l* ≤ 33	-34 ≤ *h* ≤ 34, -34 ≤ *k* ≤ 34, -34 ≤ *l* ≤ 32	-34 ≤ *h* ≤ 34, -34 ≤ *k* ≤ 34, -34 ≤ *l* ≤ 32
Reflections collected	35964	35791	35741
Independent reflections	1161 [R_{int} = 0.1312, R_{sigma} = 0.0334]	1155 [R_{int} = 0.1304, R_{sigma} = 0.0332]	1153 [R_{int} = 0.1307, R_{sigma} = 0.0332]
Data/restraints/parameters	1161/137/110	1155/105/94	1153/105/94
Goodness-of-fit on F^2	1.213	1.052	1.061
Final *R* indexes [*I*>=2σ(*I*)][a,b]	R_1 = 0.0938, wR_2 = 0.2753	R_1 = 0.0760, wR_2 = 0.2350	R_1 = 0.0809, wR_2 = 0.2391
Final *R* indexes [all data][a,b]	R_1 = 0.1101, wR_2 = 0.3036	R_1 = 0.0908, wR_2 = 0.2606	R_1 = 0.0966, wR_2 = 0.2677
Largest diff. peak/hole / e Å^{-3}	1.33/-0.48	1.12/-0.37	1.17/-0.55

[a] $R_1 = \Sigma||F_o| - |F_c||/\Sigma|F_o|$.

[b] $wR_2 = |\Sigma w(|F_o|^2 - |F_c|^2)|/\Sigma|w(F_o^2)^2|^{1/2}$.